

AUXILIARY INVERTER CONFIGURATION FOR ENERGY EFFICIENCY  
IMPROVEMENT AND COST EFFECTIVENESS OF ELECTRIC VEHICLE INVERTER

by

SAROJ SANJAY SHINDE



APPROVED BY SUPERVISORY COMMITTEE:

---

Dr. Ghanshyamsinh Gohil, Chair

---

Dr. Babak Fahimi

---

Dr. Bilal Akin

---

Dr. Poras Balsara

Copyright © 2019

SAROJ SANJAY SHINDE

All rights reserved

*To Mummy, Papa and Suraj*

AUXILIARY INVERTER CONFIGURATION FOR ENERGY EFFICIENCY  
IMPROVEMENT AND COST EFFECTIVENESS OF ELECTRIC VEHICLE INVERTER

by

SAROJ SANJAY SHINDE, BE

THESIS

Presented to the Faculty of  
The University of Texas at Dallas  
in Partial Fulfillment  
of the Requirements  
for the Degree of

MASTER OF SCIENCE IN  
ELECTRICAL ENGINEERING

THE UNIVERSITY OF TEXAS AT DALLAS

May 2019

## ACKNOWLEDGMENTS

I would like to express my sincere gratitude to my supervisor Dr.Gohil for providing me with the opportunity to work on this thesis. I am very fortunate to work under him due to his patience, continuous support and motivation. His method of approaching problems is very logical and pragmatic and this inspired me to learn and improvise. I wish to thank my graduate committee members Dr. Babak Fahimi, Dr. Poras Balsara and Dr.Bilal Akin for accepting my request and providing their time to be part of the committee.

I also want to thank my friends and colleagues at Power Electronics Lab, Saurabh Kumar, G. Veera Bharath, Anand Patel for their guidance and for helping me to improve my skills on several levels.

My earnest gratitude to my parents and my brother for their trust, continuous support and prayers during all the stages of my life, wherever I have chosen to be and whatever I have chosen to do. I am always thankful for their blessings which makes me to climb new heights. Last but not least, I am thankful to my wonderful friends and roommates, Vaibhav Pawaskar, Pranjali Hirlekar, Harshita Dekate, Neha Kaushik, Noopur Dulet, Sidharth Debnath and Ajinkya Shinde for their moral support.

April 2019

AUXILIARY INVERTER CONFIGURATION FOR ENERGY EFFICIENCY  
IMPROVEMENT AND COST EFFECTIVENESS OF ELECTRIC VEHICLE INVERTER

SAROJ SANJAY SHINDE, MS  
The University of Texas at Dallas, 2019

Supervising Professor: Dr. Ghanshyamsinh Gohil

Wide band gap (WBG) based power switches have improved the efficiency and power density in the power electronic systems. The higher cost compared to silicon switches is the road block for large scale adoption of SiC devices. In this thesis, a high efficient and cost effective inverter configuration for Electric Vehicle (EV) application is proposed where a WBG device based auxiliary inverter is used in parallel to Si-IGBT based main inverter. The auxiliary inverter assists the switching of main inverter to minimize the switching losses and at the same time to increase the cost effectiveness of the system. A detailed switching scheme is presented to achieve the mentioned features. Simulation analysis considering UDDS (City cycle) driving cycle is done to show the effectiveness of the WBG based auxiliary inverter in improving the energy efficiency of EVs.

## TABLE OF CONTENTS

ACKNOWLEDGMENTS . . . . .	v
ABSTRACT . . . . .	vi
LIST OF FIGURES . . . . .	ix
LIST OF TABLES . . . . .	xii
CHAPTER 1 INTRODUCTION . . . . .	1
1.1 Overview of electric vehicle components . . . . .	2
1.2 Previous work . . . . .	5
1.3 Thesis Outline . . . . .	6
CHAPTER 2 ELECTRIC VEHICLE . . . . .	8
2.1 Methods for vehicle modelling . . . . .	8
2.2 Power consumption of EV . . . . .	10
2.3 Motor Modelling . . . . .	19
CHAPTER 3 INVERTER MODELLING . . . . .	26
3.1 Introduction . . . . .	26
3.2 Overview of Switching Devices . . . . .	27
3.2.1 MOSFET (Metal Oxide semiconductor Field effect transistor) . . . . .	27
3.2.2 MOSFET Switching waveform . . . . .	29
3.2.3 IGBT (Insulated Gate bipolar transistor) . . . . .	32
3.2.4 IGBT switching waveform . . . . .	33
3.3 Inverter Modelling . . . . .	35
CHAPTER 4 AUXILIARY INVERTER CONFIGURATION . . . . .	42
4.1 Double Pulse Test . . . . .	42
4.2 Description of auxiliary inverter configuration . . . . .	44
4.3 Gate control strategy . . . . .	45
4.4 Validation using PLECS software . . . . .	47
4.5 Experimental Verification . . . . .	50
CHAPTER 5 CONCLUSION . . . . .	56
5.1 Summary . . . . .	56

5.2 Future Work . . . . .	57
APPENDIX COMPONENT DESCRIPTION OF DOUBLE PULSE TEST PROTO- TYPE FOR AUXILIARY INVERTER CONFIGURATION . . . . .	58
REFERENCES . . . . .	62
BIOGRAPHICAL SKETCH . . . . .	65
CURRICULUM VITAE	

## LIST OF FIGURES

1.1	Block Diagram showing basic blocks present in Plug in Electric vehicle [11] . . . . .	2
1.2	Broad Classification for Power Electronics in Electric vehicle [1] . . . . .	4
2.1	Quasi-static modelling approach where, $P_B$ = Total power requested to the battery , $P_{aux}$ = auxiliary loads, $P_{InInv}$ = Power requested by power converter, ( $P_B= P_{aux} + P_{InInv}$ ) $P_{InMot}$ = Power requested by electric machine to the power converter, $T_{EM}$ = Electric machine torque, $v, a$ = vehicular speed and acceleration, $f$ = vehicular traction force, $\Omega$ = Electric machine angular speed [11]. . . . .	8
2.2	Dynamic modelling approach where, $I_{batt}$ = Battery Current, $I_{aux}$ = auxiliary load current requested to the battery, $I_{inv}$ = Inverter current, $V_{batt}$ = Battery voltage, $I$ = Electric motor current, $V_s$ = Electric motor voltage, $T_{EM}$ = Electric machine torque, $v, a$ = vehicular speed and acceleration, $f$ = vehicular traction force, $\Omega$ = Electric machine angular speed [11]. . . . .	9
2.3	Driving Cycle : (a) City Cycle, (b) Highway cycle, (c) New york city cycle, (d) US06 cycle, (e) SC03 cycle . . . . .	11
2.4	Power consumption for different driving cycle Cycle . . . . .	15
2.5	Histogram showing distribution of power consumption by EV for city cycle . . . . .	16
2.6	Histogram showing distribution of power consumption by EV for Highway cycle . . . . .	16
2.7	Histogram showing distribution of power consumption by EV for NYCC cycle . . . . .	17
2.8	Histogram showing distribution of power consumption by EV for US06 cycle . . . . .	17
2.9	Histogram showing distribution of power consumption by EV for SC03 cycle . . . . .	18
2.10	Operating Points of EV motor for city Cycle . . . . .	22
2.11	Operating Points of EV motor for highway cycle . . . . .	23
2.12	Operating Points of EV motor for NYCC cycle . . . . .	23
2.13	Operating Points of EV motor for US06 Cycle . . . . .	24
2.14	Operating Points of EV motor for SC03 Cycle . . . . .	24
2.15	Torque required by EV motor for different driving cycles . . . . .	25
3.1	Power MOSFET structural view . . . . .	28
3.2	MOSFET symbol considering the parasitic capacitance's present in MOSFET [14] . . . . .	28
3.3	MOSFET turn on switching waveform considering ideal free wheeling diode [14] . . . . .	30
3.4	MOSFET turn off switching waveform considering ideal free wheeling diode [14] . . . . .	30

3.5	MOSFET switching waveform with non-ideal free wheeling diode [14]. . . . .	31
3.6	IGBT structure [14] . . . . .	33
3.7	Detailed explanation for IGBT turn on process [14] . . . . .	34
3.8	Detailed explanation for IGBT turn off process [14] . . . . .	35
4.1	Double Pulse test for GaN switch for power loss calculation . . . . .	43
4.2	Double Pulse test for GaN switch for turn on loss . . . . .	43
4.3	Double Pulse test for GaN switch for power loss calculation . . . . .	44
4.4	Block diagram of auxiliary WBG based inverter with Si based main inverter. .	45
4.5	Gate control strategy . . . . .	46
4.6	Full Bridge inverter loss calculation using PLECS software for only Si IGBT based inverter . . . . .	48
4.7	Double Pulse test (DPT) prototype. S1 and S2 are Si IGBT and WBG devices respectively, Vdc is DC source . . . . .	51
4.8	Double Pulse test (DPT) prototype. 1. and 2. 12 volts and 5 volts power supply respectively, 3. Isolated DC-DC converter for 12 volts to 15/-5 volts supply, 4. Isolated DC-DC converter for 5 volts to 9 volts supply, 5. Top IGBT switch, 6. Bottom IGBT switch, 7. GaN switch, 8. shunt resistor for current measurement through GaN switch, 9. shunt resistor for current measurement through IGBT switch, 11 and 12. positive and negative DC bus supply, 13. DC link capacitor	52
4.9	Drain Current with turn on period of 48 $\mu$ S . . . . .	53
4.10	Drain voltage with turn on period of 48 $\mu$ S . . . . .	53
4.11	Drain current and drain voltage at turn on duration . . . . .	54
4.12	Drain current and drain voltage at turn off duration . . . . .	54
4.13	IGBT turn on waveform for 50A inductor current . . . . .	55
4.14	IGBT turn off waveform for 50A inductor current . . . . .	55
A.1	Double Pulse test (DPT) prototype. 1. and 2. 12 volts and 5 volts power supply respectively, 3. Isolated DC-DC converter for 12 volts to 15/-5 volts supply, 4. Isolated DC-DC converter for 5 volts to 9 volts supply, 5. Top IGBT switch, 6. Bottom IGBT switch, 7. GaN switch, 8. shunt resistor for current measurement through GaN switch, 9. shunt resistor for current measurement through IGBT switch, 11 and 12. positive and negative DC bus supply, 13. DC link capacitor	58
A.2	Test set arrangement. 1. Double pulse test prototype, 2. Function generator, 3. Oscilloscope, 4. Power supply for gate driver part, 5. Load inductor, 6. 400 Volts DC power supply . . . . .	59

A.3 DPT prototype for auxiliary inverter bottom view . . . . .	60
A.4 DPT prototype for auxiliary inverter configuration side view . . . . .	61

## LIST OF TABLES

2.1	Vehicle (Nissan Leaf 2012 model) specification for power consumption model . . . . .	12
2.2	Motor (Nissan Leaf 2012 model) specification for motor modelling . . . . .	14
3.1	Material Properties of silicon, GaN and SiC [2] . . . . .	35
4.1	PLECS simulation loss comparison considering R-L load for one operating point	49
4.2	Energy efficiency comparison of different inverter configurations considering city cycle . . . . .	49
4.3	Cost of switching devices with almost 60 A continuous current rating which is used in main inverter . . . . .	49
4.4	Turn On and turn OFF energy for IGBT at different loading condition considering 640 $\mu$ H inductor and 400 V input DC supply . . . . .	52

# CHAPTER 1

## INTRODUCTION

Transportation sector consumes approximately 27% of total world primary energy consumption and it is second largest source for green house emission with 34% of total CO<sub>2</sub> emission [5]. A Large part of world's population use vehicles for personal transportation. After the invention of petroleum engines, vehicles have been essential part of modern life. Petroleum products have many advantages. For example, energy density of petroleum products is higher compared to batteries. Refueling the fuel tank is much easier and less time consuming than charging batteries. The driving range of petroleum-based vehicle is greater than battery-based vehicle. Similarly, Electric Vehicles (EVs) also have many advantages. For example, regenerative braking is present in EVs but not in conventional vehicles, greater energy efficiency can be achieved through on-board electric drives, the possibility to obtain electrical input from renewable sources [5], the tank-to-wheel efficiency of a conventional vehicle is almost 20 % which is much less compared to 70-90 % of EV (depending upon drive cycle), it costs almost 3.50 \$/gallon (12 cents/mile) for conventional vehicles which is much more than 0.12 \$/kWh (2 cents/mile) for EV [1]. But the serious threat of environmental pollution is produced to a large extent by CO<sub>2</sub> emission from IC engine-based vehicles and also fossil based resources are running out. Considering the pros and cons of petroleum products, researchers are looking for alternatives with greener energy technology in the sector of transportation [9].

To reduce the dependency on crude oil, efforts are being taken to replace petroleum dependent vehicles with EVs, which is a significant move towards the sustainable and environmental friendly options. The huge potential benefits of EVs have created significant interest and investment in EV technology. Because of this, they are gaining more penetration in the market particularly in city areas where air quality is a major problem and developing inclination of researchers for increasing their efficiency.

Energy conservation, emission reduction and oil supply security etc. can be ensured by using EV over conventional vehicle. Famous automobile companies are giving great importance to the development of EVs and also developed countries do not hesitate to invest in research and development of pure EV technology [29].

### 1.1 Overview of electric vehicle components

Fig. 1.1 provide overview of different components present in EV such as pilot (driver), electric machine, energy storage system, mechanical transmission system, auxiliary loads, cooling system, vehicle dynamic model and power electronics subsystems consisting of inverter, DC/DC converters, rectifiers, energy and battery management system.

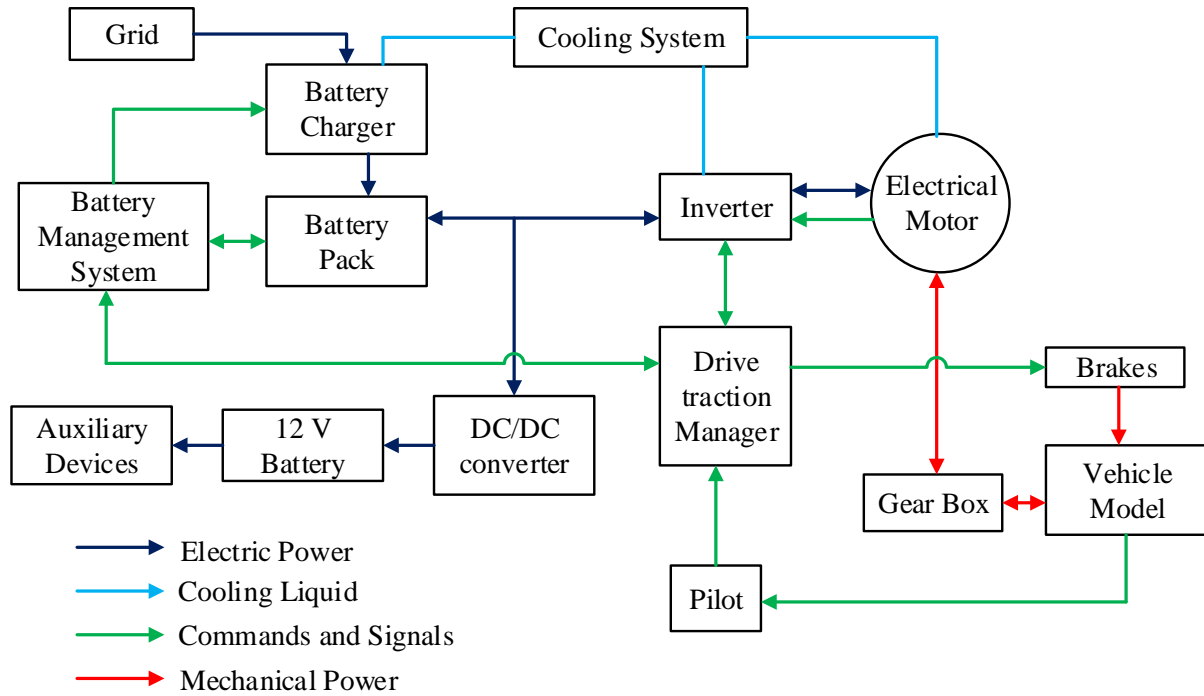


Figure 1.1: Block Diagram showing basic blocks present in Plug in Electric vehicle [11]

Electric machines contains rotating magnetic field which transfers energy from mechanical domain into electrical domain and vice versa. A machine which converts electrical energy at

input terminal into required mechanical energy at output is called motor and when energy flow is reversed it is called generator. Machines are essential for generating required torque and speed with high efficiency in wide operating range. Permanent magnet synchronous motor (PMSM), Induction motor (IM), switched reluctance motor are most commonly used machines. PMSM is 3-phase AC machine with high efficiency, high torque characteristics which is mostly used in EVs like Nissan Leaf. IM is also 3 phase AC machine with simple and robust construction with wide speed range but less efficient than PM motors which is used in Tesla, Toyota RAV-4 etc. Switched reluctance motor is DC machine which is not yet widely used in EVs because of high cost but it is capable of extreme high speed.

In general, electric motors used should have following characteristics:

- High efficiency in wide operating range
- High torque output at low speed
- Wide speed range including constant torque and constant power regions
- High reliability and robustness for various vehicle operating conditions
- Reasonable cost

In this thesis PMSM is selected for energy efficiency analysis. It is popular due to its high efficiency, low inertia, high steady state torque density, simple control and cheaper power electronics associated with control [25]. It can be categorized on basis of magnet arrangement in rotor: internal mounted magnets (IM) and surface mounted magnets (SM). The SM have fixed reluctance at any rotor angle and therefore have uniform air gap with equal magnetizing inductance for both direct and quadrature axis ( $L_d$  and  $L_q$ ). While IM have variable magnetizing inductance which varies with rotor angle.

Field oriented control of PMSM is widely used as vector control method. The aim of FOC is to control d,q components of stator currents or consequently the fluxes of motor to

produce required magnetic field and torque. The main advantage is fast response and little ripple [25].

Power electronics systems are key components in EVs. They are used to process and control the flow of electric energy by supplying voltages and current in a form that is optimally suited for loads [14]. As discussed previously, EV mainly contains inverter, DC-DC converters, rectifiers, and other power electronics systems as shown in Fig. 1.2. Converters have duty of transforming electric power of particular voltage-current into required level and 3 phase inverter is used to convert electric energy from DC voltage, (supplied through energy storage system) to the load (Electric motor) or vice versa during retardation [20].

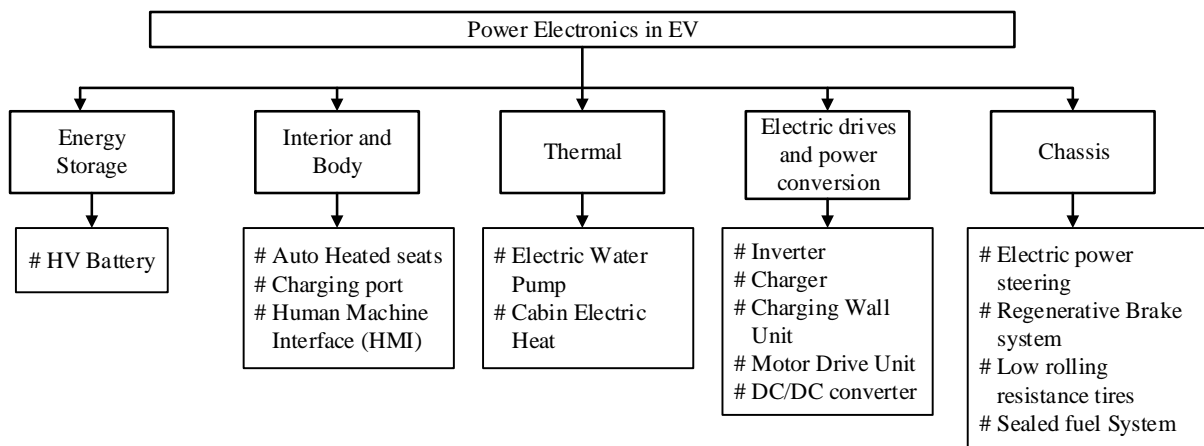


Figure 1.2: Broad Classification for Power Electronics in Electric vehicle [1]

Energy Management system (EMS) uses hardware and software control for optimization of energy efficiency and drivability. Energy storage systems could be battery, ultra-capacitors or fuel cells. Batteries used can be Lead-acid, Nickel-metal hydride or Lithium ion [29].

Electrification of transportation is enabling technology for safe, reliable and environmental friendly future. Therefore, intelligent and comprehensive design of power electronics is necessary to continue development of EVs [1]. Considering the state of art, there are

different problems associated with power electronics for advanced vehicle applications which are given below:

1. Low efficiency at light load conditions for inverters and converters
2. High cost of devices and power modules especially for wide band gap (WBG) and advanced silicon devices.
3. Low current density and device scaling issues for high power converters.
4. Low power density for the low voltage electronics.

## **1.2 Previous work**

Inverter, electric motor and battery are basic parts of EV. Use of new material for power electronic devices, new/ modified inverter topologies or with improved control strategy, efficiency of inverter can be improved. Since the efficiency of motor and inverter is already high and hence efficiency improvement achieved through different solutions will not be that much significant, but the power stored in the battery which is the most expensive part in EV should be used with supreme care [7].

Considerable research in the field of power electronics, related to different inverter topologies, DC bus voltage levels, inverter switching frequencies is being analyzed for EV inverters [20]. New wide band gap (WBG) devices like Silicon Carbide (SiC) MOSFETs and Gallium Nitride (GaN) have emerged and research is going on to investigate its implementation in vehicular applications for efficient and cost effective methods. For this, it is important to first characterize SiC and GaN devices since its characterization is different than Silicon (Si) based Insulated Gate Bipolar Transistor (IGBT). In [16], [17], [18] characterization of Schottky diode, Si IGBT, SiC MOSFETs and GaN devices has been explained.

Out of several benefits, absence of PN junction in SiC MOSFET, is advantageous over Si IGBT. Paralleling of devices with non existence of PN junction can reduce the conduction loss effectively, but it can cause mismatch in on-state resistance. Mismatch in PCB layout in parallel configuration can cause difference in stray inductance in gate or power loop leading to unbalanced dynamic behaviour during switching. But this dissimilarities does not hamper the use of paralleling of devices . Literature survey has been carried out for characterizing different types of switches in parallel manner. Similar to paralleling of individual switches the paralleling of inverter is also possible. Paralleling of inverter in Photo-Voltaic (PV) sector is mainly done to supply back up power whenever necessary or even during high power requirement.

Loss calculation in inverter is discussed in [28], but it is not put it into vehicular content. The impact of using Si IGBT, SiC MOSFET and GaN in EV based inverter is also important. For calculating their impact, it is first required to model the EV. Some of this literature [11], [27] have discussed the modelling of EV. In thesis [19], loss calculation of devices in vehicular content is done and it is also shown that 1.5% of improvement in drive cycle efficiency can be achieved by replacing Si freewheeling diode with SiC diode and 2 to 5 % drive cycle efficiency in New European Driving Cycle (NEDC) can be achieved by changing Si IGBT with SiC MOSFET. One of the drawback of modelling EV inverter with only SiC device is increased cost of inverter thus, cost effective and energy efficient EV inverter is proposed in this thesis. This is achieved through use of auxiliary inverter configuration in parallel to main inverter, which will be used during low load current requirement and assisting the main inverter for switching during high power requirement.

### **1.3 Thesis Outline**

Chapter 1 discusses the state of art and basic electrical overview of electric vehicle.

In Chapter 2, description of EV power consumption profile along with different approaches for EV and machine modelling is discussed.

Chapter 3 presents the basics of different switching devices with its switching characteristics. Also, inverter modelling considering the switching and conduction loss for switching devices is described.

Chapter 4, discusses the concept of using an auxiliary inverter in parallel to the main inverter along with different possible modes of operation. Also, the comparative study in terms of efficiency and cost effectiveness of the proposed scheme with respect to the conventional inverters is presented followed by the conclusion in chapter 5. The construction details of prototype for auxiliary inverter configuration is explained in appendix.

## CHAPTER 2

### ELECTRIC VEHICLE

#### 2.1 Methods for vehicle modelling

A complete block model for EV based system as shown in Fig. 1.1 can be designed using two different approaches, namely reverse and forward approach [5], [11]. The block diagram for this approaches are shown in Fig. 2.1 and 2.2 respectively.

##### 1. Reverse approach (Quasi-static approach)

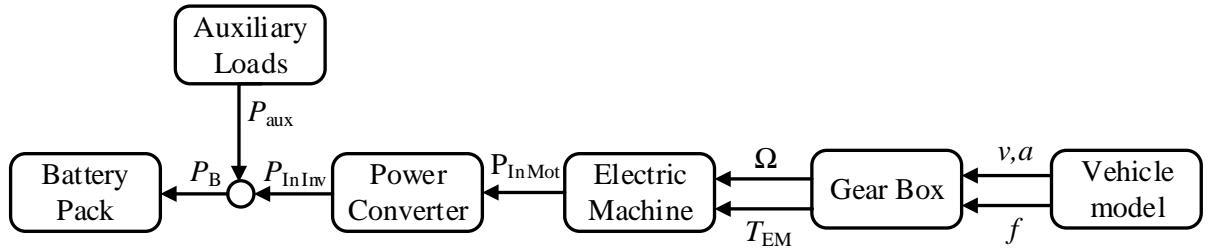


Figure 2.1: Quasi-static modelling approach where,  $P_B$  = Total power requested to the battery ,  $P_{aux}$ = auxiliary loads,  $P_{InInv}$ = Power requested by power converter, ( $P_B = P_{aux} + P_{InInv}$ )  $P_{InMot}$ = Power requested by electric machine to the power converter,  $T_{EM}$ = Electric machine torque,  $v, a$ = vehicular speed and acceleration,  $f$ = vehicular traction force,  $\Omega$ = Electric machine angular speed [11].

The models which calculates tractive force at wheels and then work backwards is reverse approach. Using input variables such as vehicular speed and acceleration of EV and solving equation going backwards block by block as shown in Fig. 2.1. Some of the advantages and disadvantages of reverse approach are discussed below:

- These models are used were less computational time is required.
- Flexible for simulating large number of driving cycles.
- The information flow is unidirectional and equation set is simpler making the system reliable which can be implemented in MATLAB environment, but one of the drawback of such system is less accuracy than dynamic approach.

- This approach does not consider the real time response and constrain of power train components.

## 2. Forward approach (Dynamic approach)

Models which starts from engine and work with transmitted and reflected torque is forward model. Each sub component is connected with previous and next blocks using interconnected variables. Interleaved connection of sub models influences the behaviour of total system as shown in Fig. 2.2.

- Dynamic approach generates response that runs forward the complete model, influencing the output of following sub-models which makes it possible to study total behaviour with physical limits of each components.
- High computational efforts are required for this approach and therefore execution time slow.
- Results obtained through this approach are more accurate.

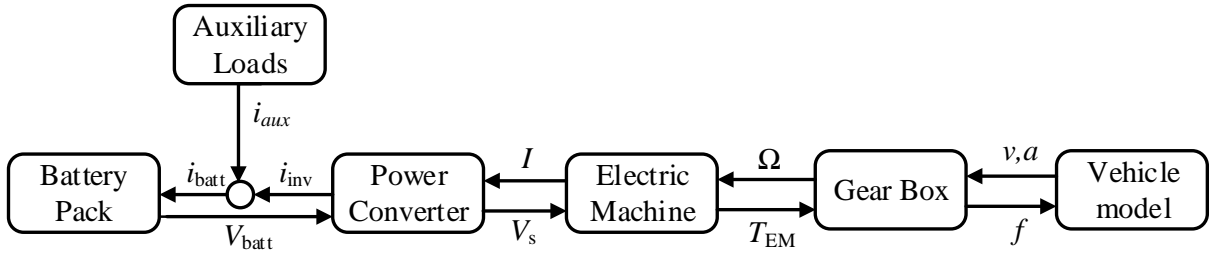


Figure 2.2: Dynamic modelling approach where,  $I_{\text{batt}}$  = Battery Current,  $I_{\text{aux}}$ = auxiliary load current requested to the battery,  $I_{\text{inv}}$ = Inverter current,  $V_{\text{batt}}$ = Battery voltage,  $I$ = Electric motor current,  $V_s$ = Electric motor voltage,  $T_{\text{EM}}$ = Electric machine torque,  $v, a$ = vehicular speed and acceleration,  $f$ = vehicular traction force,  $\Omega$ = Electric machine angular speed [11].

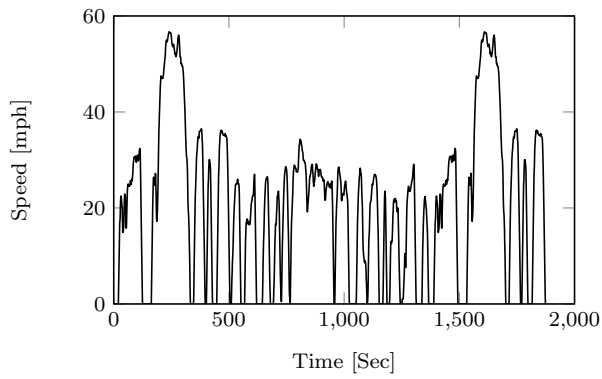
## 2.2 Power consumption of EV

EVs are gaining significant market and development in this field will appreciably reduce consumption of fuel and  $CO_2$  emission levels. Different studies have been performed and predicted that use of EV will significantly increase in upcoming years. Such as, a study performed by University of California, Berkeley predicted that approximately 2.5 million EVs will be present on American roads by 2020 [5].

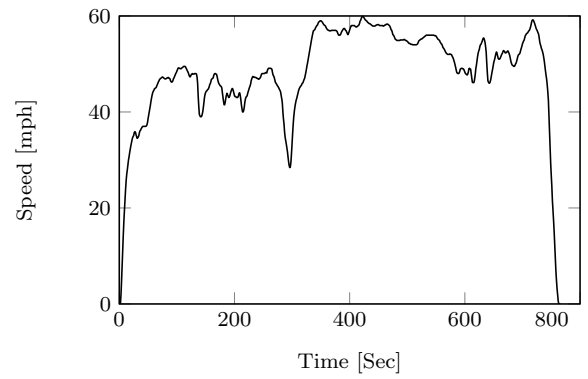
To understand the distribution of energy consumption by EV over the the different driving cycles, simple and precise model is needed which will calculate energy consumption over the complete driving cycle. Literature is available for developing energy consumption model for EV. In [5], [6], [26] mathematical model is proposed to calculate instantaneous electric power consumption of EV which considers instantaneous braking energy and regeneration as a function of vehicle deceleration. A regenerative braking system of EV, permits for recovery of braking energy from electric motor which acts as generator during deceleration and this recovered energy is stored in battery system. Due to presence of regenerative braking in EVs, they were found to be much more efficient in urban routes than uninterrupted freeways which is opposite to that of internal combustion engine (ICE) based vehicles since they exert more energy in urban driving cycles.

Based on the driving cycle, the power consumption profile varies. Therefore, computation and estimation of EV power consumption is required for future improvement in energy efficiency which can also be used for optimization the cost [26]. There are many types of driving cycles referred around the world. Following are some of the Advanced Vehicle Testing Activity (AVTA) data for driving cycles provided by United States Environmental Protection Agency (US EPA) as shown in Fig. 2.3 [24]:

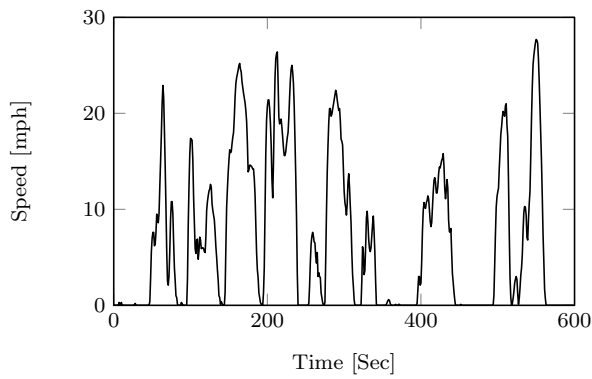
- UDDS/LA4 (The city test or Urban Dynamometer Driving Schedule)
- HWFET (Highway Fuel Economy Driving Schedule)



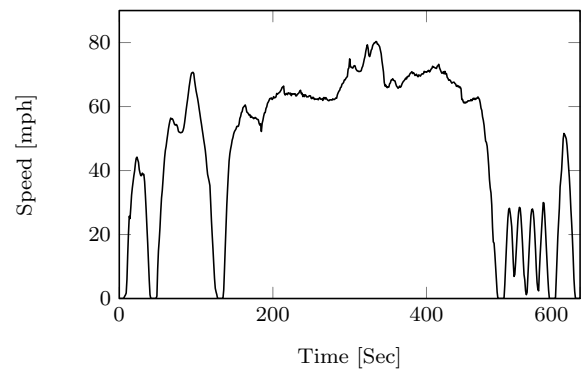
(a) City Cycle



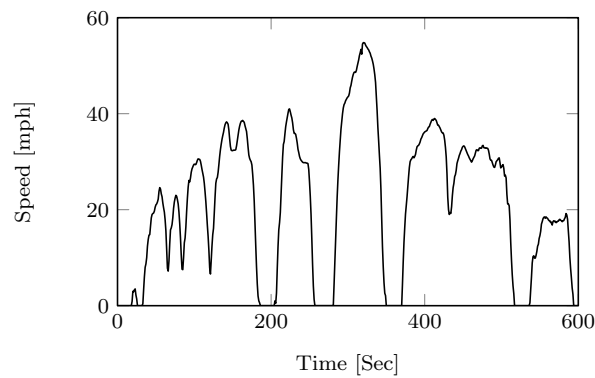
(b) Highway Cycle



(c) NYCC



(d) US06



(e) SC03

Figure 2.3: Driving Cycle : (a) City Cycle, (b) Highway cycle, (c) New york city cycle, (d) US06 cycle, (e) SC03 cycle

- NYCC (The New York city cycle)
- US06 (High acceleration aggressive driving schedule / Supplemental FTP driving schedule)
- SC03 (Air conditioning supplemental FTP driving schedule)

The Comprehensive Power-based EV energy consumption Model (CPEM), backward model is used for estimating energy consumption based on drive cycle and vehicle characteristics, where instantaneous speed of vehicle and vehicle characteristics are used as input variable [5]. The vehicle model used can be standardized using publicly available data of EV without any field data collection.

Table 2.1: Vehicle (Nissan Leaf 2012 model) specification for power consumption model

<b>Parameter</b>	<b>Symbol</b>	<b>Nissan leaf</b>
Vehicle mass	$m$	1521 kg
Vehicle top speed	$v_{max}$	140 km/h
Frontal area of vehicle	$A_f$	2.3316 ( $m^2$ )
Aerodynamic drag coefficient	$C_D$	0.28
Rolling resistance	$C_r$	1.75
	$c_1$	0.0328
	$c_2$	4.575
Gear ratio	-	7.789
Maximum output power	$P_{MotMax}$	80 kW
Maximum Torque	$T_{Max}$	280 N-m
Wheel Radius	$r_w$	0.28 m
Battery Type	-	Laminated type thin lithium ion battery
Battery storage	-	24 kwh
Battery voltage	$V_{batt}$	385 V
Drive-line efficiency	$\eta_{DL}$	92 %
Battery efficiency	$\eta_{BAT}$	90 %
Electric motor efficiency	$\eta_{EM}$	91 %
Auxiliary Load	$P_{Aux}$	700 W

For this research, NISSAN Leaf (2012) data is used for power consumption calculation. This vehicle is selected due to its popularity in EV market and lot of data with detailed specifications is available, also lot of research laboratories have published experimental data. The vehicle and motor specification used in this research is provided in the Table 2.1 and Table 2.2 respectively.

The following formula is used to calculate the power at wheels, [6].

$$P_w(t) = \{ma(t) + mg \cdot \cos(\theta) \frac{C_r}{1000} [c_1 v(t) + c_2] + \frac{1}{2} \rho_{Air} A_f C_D v^2(t) + mg \cdot \sin(\theta)\} \cdot v(t) \quad (2.1)$$

Where,

$m$  = Vehicle mass

$a(t)$  = Acceleration / deceleration of vehicle  $\left(\frac{m}{s^2}\right)$ ,

$g$  = Gravitational acceleration  $\left(\frac{m}{s^2}\right)$ ,

$C_r, c_1, c_2$  = Rolling resistance constant which depends upon

road surface type, road condition and vehicle tyre type,

$v(t)$  = Vehicle speed  $\left(\frac{m}{s}\right)$ ,

$\rho_{Air}$  = Air mass density  $\left(\frac{kg}{m^3}\right)$ ,

$A_f$  = Frontal area of vehicle  $\left(\frac{m^2}{s^2}\right)$ ,

$C_D$  = Aerodynamic drag coefficient,

$\theta$  = Road angle (Assumed zero),

The power necessary for traction, is given as,

$$P_T(t) = \begin{cases} \frac{P_W(t) + P_{Aux}}{\eta_{DL} \cdot \eta_{EM} \cdot \eta_{BAT}}, & \text{if } P_W(t) \geq 0 \\ [P_W(t) + P_{Aux}] \cdot (\eta_{DL} \cdot \eta_{EM} \cdot \eta_{BAT}) \cdot \eta_{RB}(t), & \text{if } P_W(t) < 0 \end{cases} \quad (2.2)$$

Where,

$P_W(t)$  = Power at wheels,

$P_{Aux}$  = Power of auxiliary system,

$\eta_{DL}$  = Drive-line efficiency,

$\eta_{EM}$  = Motor efficiency,

$\eta_{BAT}$  = Battery efficiency,

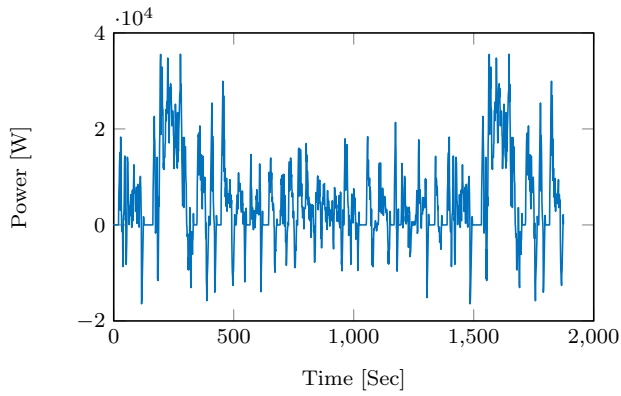
$\eta_{RB}$  = Regenerative braking efficiency,

$$\eta_{RB} = \begin{cases} e^{\frac{\alpha}{|\alpha(t)|}}, & \text{if } a(t) < 0 \\ 0, & \text{if } a(t) \geq 0 \end{cases} \quad (2.3)$$

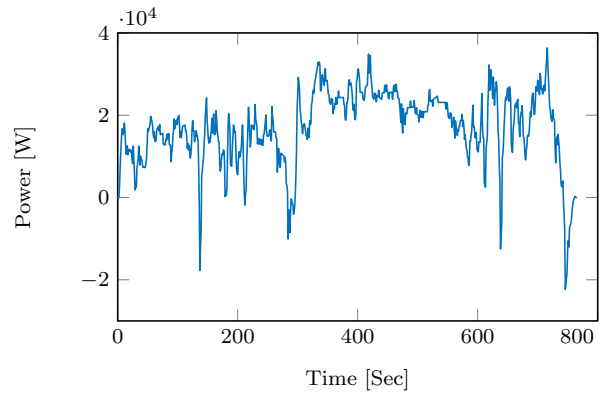
Alpha depends upon electric vehicle specification, usually in range of [0,1]. The power at electric motor ( $P_{electricmotor}(t)$ ) is computed, considering drive-line efficiency and electric motor efficiency as  $\eta_{DL}= 91\%$ . Since the reported Nissan Leaf motor efficiency is about 85% to 95%, therefore considering 91% minimizes the average error between empirical data and estimated energy consumption values. In addition power consumed by auxiliary system is considered as 700 W [5].

Table 2.2: Motor (Nissan Leaf 2012 model) specification for motor modelling

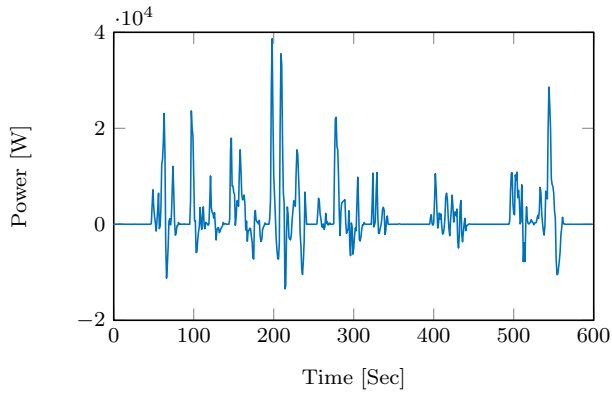
Parameter	Symbol	Nissan leaf
Motor Type	-	PMSM
Top motor speed	-	10390 rpm
Stator resistance	$R_s$	0.0143 $\Omega$
Motor Pole Pair	n	4
Stator Inductance	$L_d$	800e-6 $H$
Stator Inductance	$L_q$	800e-6 $H$
Permanent magnet flux	$\phi_m$	0.0523
Motor weight	-	58 kg



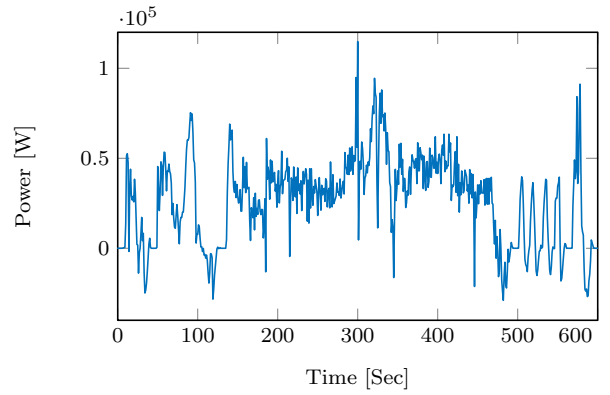
(a) Power graph for City cycle



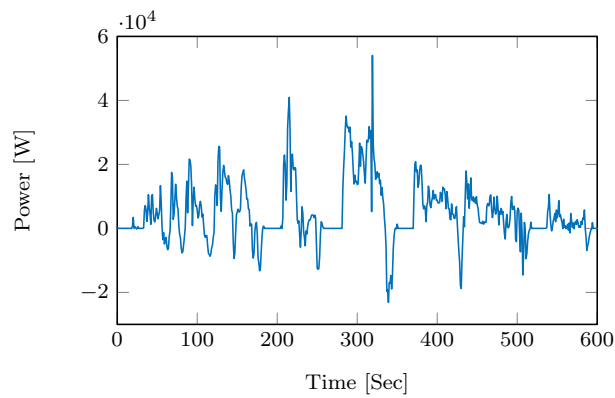
(b) Power graph for Highway cycle



(c) Power graph for NYCC cycle



(d) Power graph for US06 cycle



(e) Power graph for SC03 cycle

Figure 2.4: Power consumption for different driving cycle Cycle

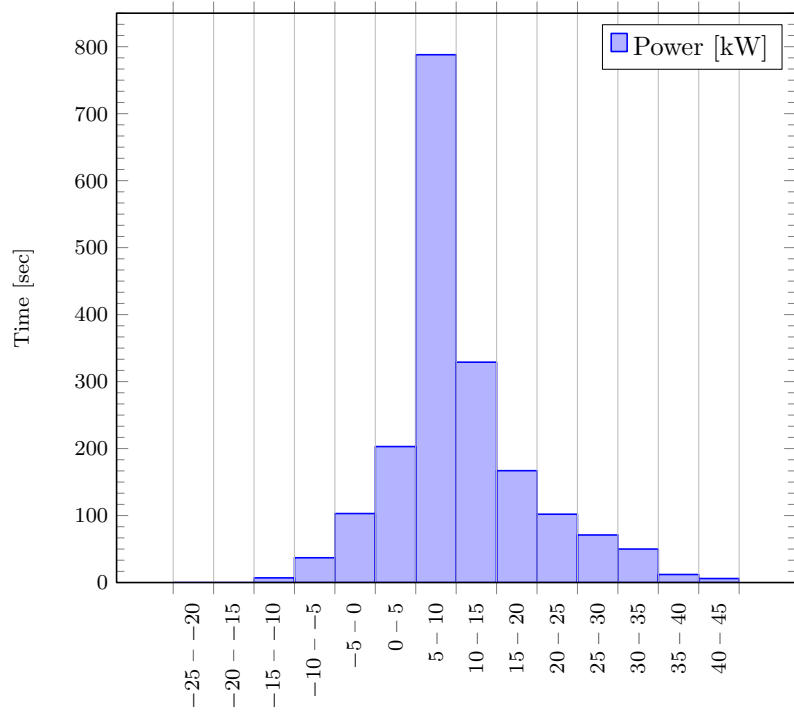


Figure 2.5: Histogram showing distribution of power consumption by EV for city cycle

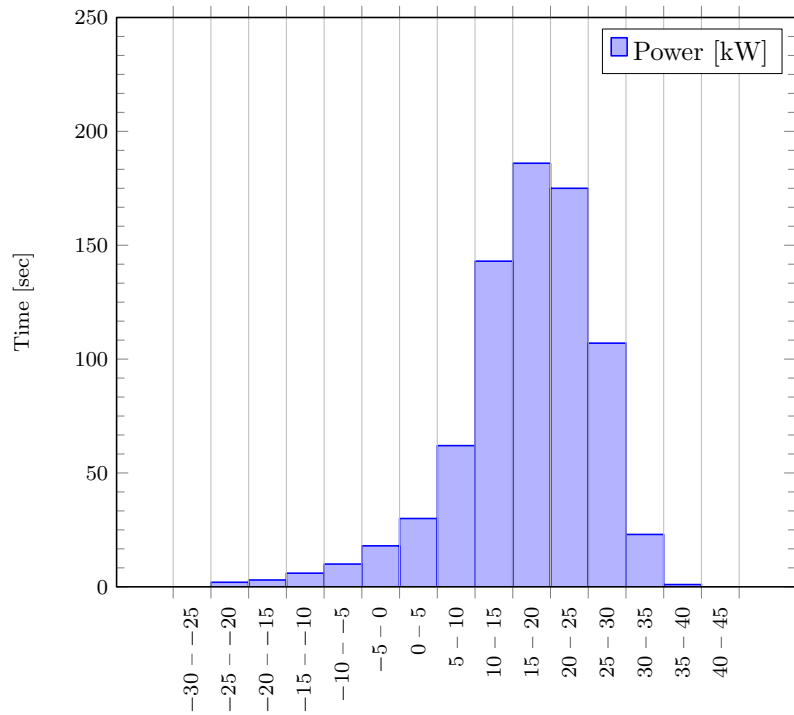


Figure 2.6: Histogram showing distribution of power consumption by EV for Highway cycle

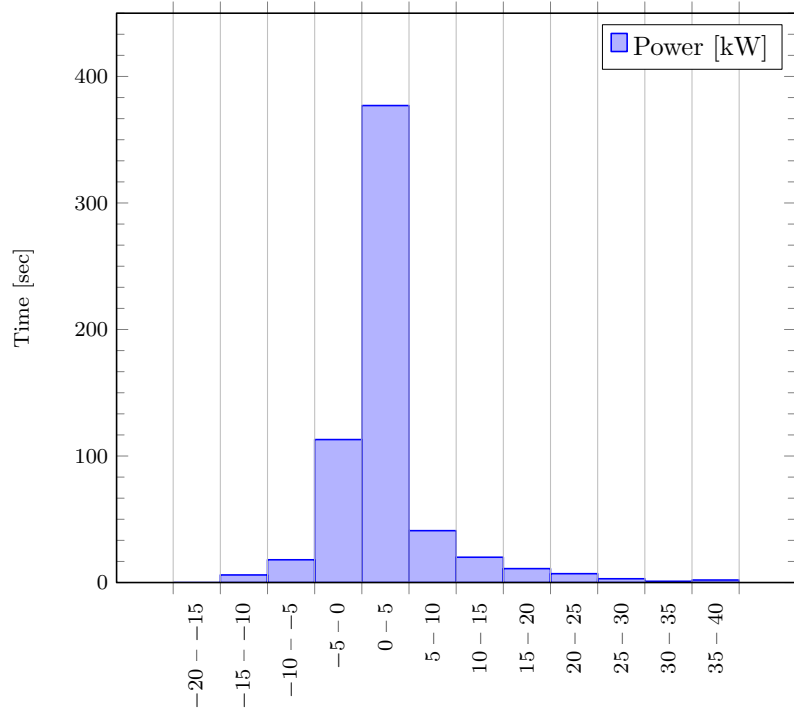


Figure 2.7: Histogram showing distribution of power consumption by EV for NYCC cycle

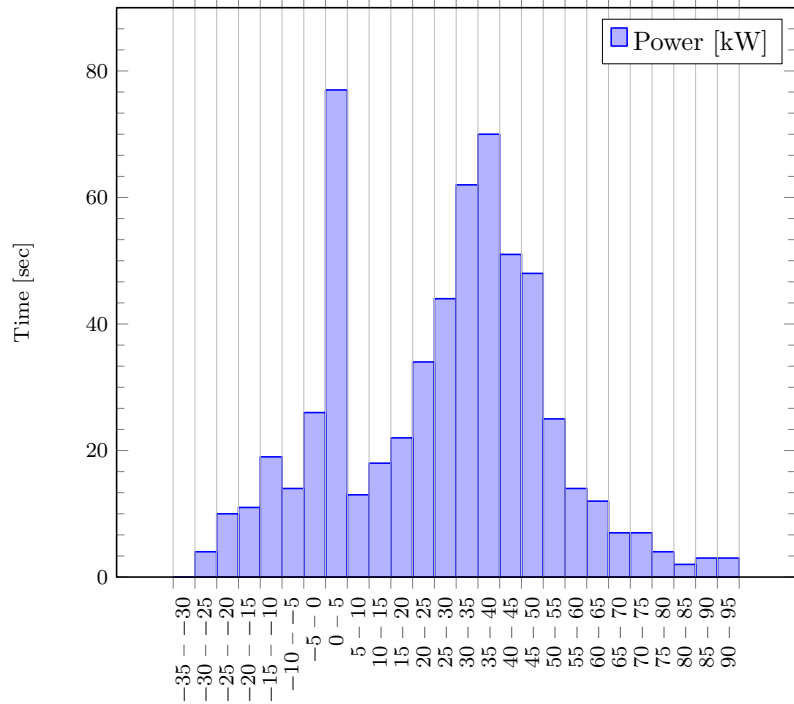


Figure 2.8: Histogram showing distribution of power consumption by EV for US06 cycle

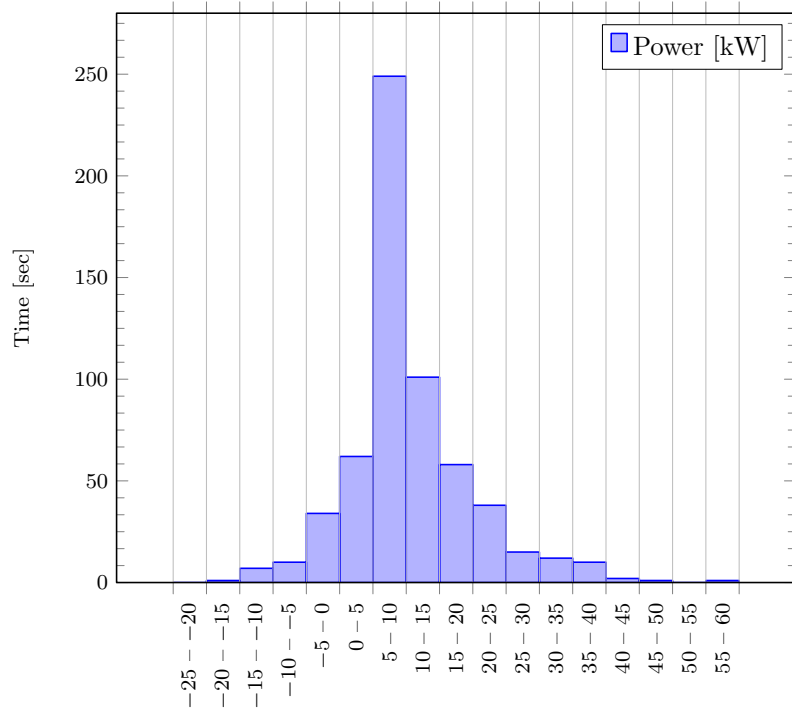


Figure 2.9: Histogram showing distribution of power consumption by EV for SC03 cycle

By using vehicle model provided in [26], the power consumption for NISSAN leaf is calculated for different driving cycles which are shown in Fig. 2.4. Fig. 2.5 to 2.9 provides the histogram showing the power consumption of EV with respect to the time duration within the cycle period. From the figures, it can be interpreted that EV draws full rated power only for small duration of time.

In case of city cycle, the power consumption of EV is between 0-5 kW for almost 35 to 40 % of total time during driving cycle. Similarly, it can be seen in supplemental FTP cycle. For highway fuel economy driving cycle, 10 to 15 kW of power is required for about 30 to 35 % of total time during given driving cycle which is little higher than city cycle. Thus it can be concluded that, EV operates at much lesser power than the rated power for maximum duration of time.

## 2.3 Motor Modelling

The following section describes component by component simplified dynamic approach for motor modelling. For EV energy efficiency and loss calculation, detailed motor modelling including electromechanical dynamic is not required and controlled motor with steady state model including energetic phenomenon is sufficient. In this section the mathematical modelling of PMSM is referred from paper [11], [27] as shown below.

Backward approach is employed for the electric motor model and starting from required torque and motor angular speed, the  $v_s$  and  $i_s$  is determined. First it should be checked whether the required torque ( $T_{ref}$ ) is in specified limit and not exceeding the maximum torque ( $T_{refMax}$ ) limit and also consequent power ( $T_{ref} \cdot \Omega$ ) request should not exceed maximum power limit ( $P_{motMax}$ ), which is verified by using equation 2.4

$$\left\{ \begin{array}{l} T_{ref} = T_{refMax}, \quad \text{if } T_{ref} > T_{refMax} \\ T_{ref} = \frac{P_{motMax}}{\Omega}, \quad \text{if } T_{ref} \cdot \Omega > T_{refMax} \end{array} \right\} \quad (2.4)$$

where,  $\Omega$  = Mechanical angular speed,

Additionally the field weakening condition has to be imposed to the PMSM and accordingly the correct value of  $I_d$  should be calculated, as shown in equation 2.5. In constant torque/flux region the value of  $I_d$  current can be considered as zero but in field weakening region it should be imposed as negative.

$$\left\{ \begin{array}{l} \psi_s = \frac{\psi_m \Omega_n}{\Omega}, \quad \text{if } \Omega > \Omega_n \\ \psi_s = \psi_m, \quad \text{if } \Omega < \Omega_n \\ I_d = \frac{\psi_s - \psi_m}{L_s} \end{array} \right\} \quad (2.5)$$

where,

$\psi_m$  = Permanent Magnet rated flux,

$\psi_s$  = Resultant rotor flux,

$\Omega_n$  = Rated speed,

$I_d$  and  $I_q$  = stator phasor current components,

$L_s$  = stator synchronous inductance,

Equations 2.6, 2.7, 2.8 are used to calculate the motor quantities with considering

$T_{EM} = T_{ref}$  and  $\Omega$

$$\left\{ \begin{array}{l} V_d = R_s I_d - \omega L_s I_q \\ V_q = R_s I_q - \omega L_s I_d + \omega \cdot \psi_m \end{array} \right\} \quad (2.6)$$

$$\left\{ \begin{array}{l} T_{EM} = n \psi_m I_q \\ \Omega = \frac{\omega}{n} \end{array} \right\} \quad (2.7)$$

Where,

$V_d$  and  $V_q$  = stator voltage phasors,

$R_s$  = Stator resistance,

$\omega$  = AC variable angular frequency,

$n$  = pole pair numbers,

The copper and iron losses are calculated as shown in equation 2.8, where  $P_{Fen}$  is iron loss at rated flux and speed with electric pulsation, considering that they are directly

proportional to speed  $\omega$  and inversely proportional to square of the flux magnitude [12], [27].

$$\left\{ \begin{array}{l} P_{Cu} = R_s I_d^2 + R_s I_q^2 \\ P_{Fe} = P_{Fen} \frac{\omega}{\omega_n} \\ P_m = T_{EM} \Omega \\ P_{LossMot} = P_{Cu} + P_{Fe} \\ P_{InMot} = P_m + P_{LossMot} \end{array} \right\} \quad (2.8)$$

$$\left\{ \begin{array}{l} I_s = \sqrt{I_d^2 + I_q^2} \\ V_s = \sqrt{V_d^2 + V_q^2} \\ Q_{InMot} = V_d I_d + V_q I_q \\ \phi = \tan^{-1} \left( \frac{Q_{InMot}}{P_{InMot}} \right) \end{array} \right\} \quad (2.9)$$

Furthermore the following conditions are considered for global electrical drive limits which are imposed to examine that the requested condition do not exceed the allowed conditions.

1. Maximum RMS input current  $I_{max}$  is related to inverter current limit, equation 2.10

$$I = \frac{I_s}{\sqrt{3}} < I_{max} \quad (2.10)$$

If the above condition is not met than reduce  $T_{ref}$  and solve equation 2.6 to 2.9.

2. Maximum motor voltage limit  $V_{sMax}$ , corresponds to maximum deliverable inverter voltage for a given battery voltage, equation 2.11

$$V_s < V_{sMax} \quad \text{where} \quad V_{sMax} = \frac{V_{batt}}{\sqrt{2}} \quad (2.11)$$

If the amplitude of stator voltage exceeds the limit of inverter voltage, which can be produced with the available battery voltage  $V_{batt}$  then the flux value  $\phi_s$  is reduced till  $V_s < V_{sMax}$  and than again solve equation 2.6 to 2.9.

3. Maximum motor input power limit  $P_{inMax}$  is related to maximum battery deliverable power, equation 2.12

$$P_{inMot} < P_{inMax} \quad (2.12)$$

If the above condition is not met than reduce  $T_{ref}$  and solve equation 2.6 to 2.9.

For the city driving cycle (UDDS), the corresponding motor operating points and required torque are shown in Fig. 2.10 to 2.15

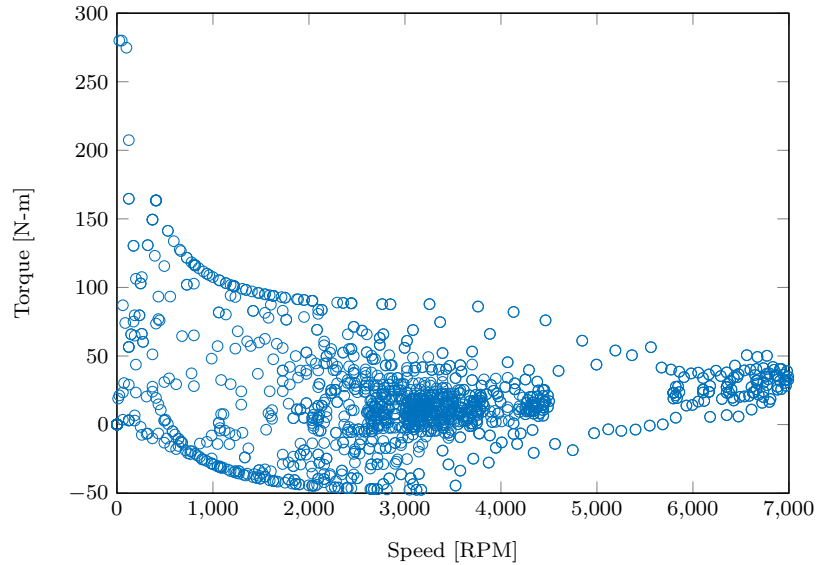


Figure 2.10: Operating Points of EV motor for city Cycle

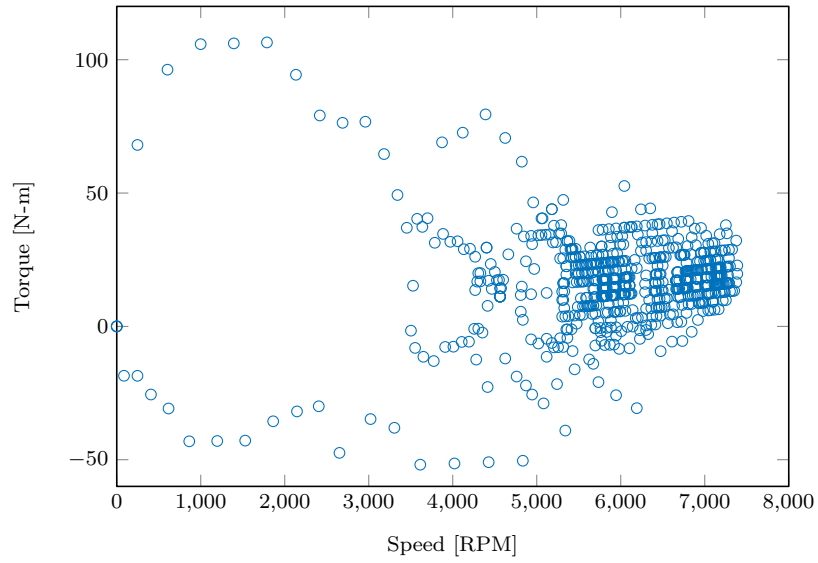


Figure 2.11: Operating Points of EV motor for highway cycle

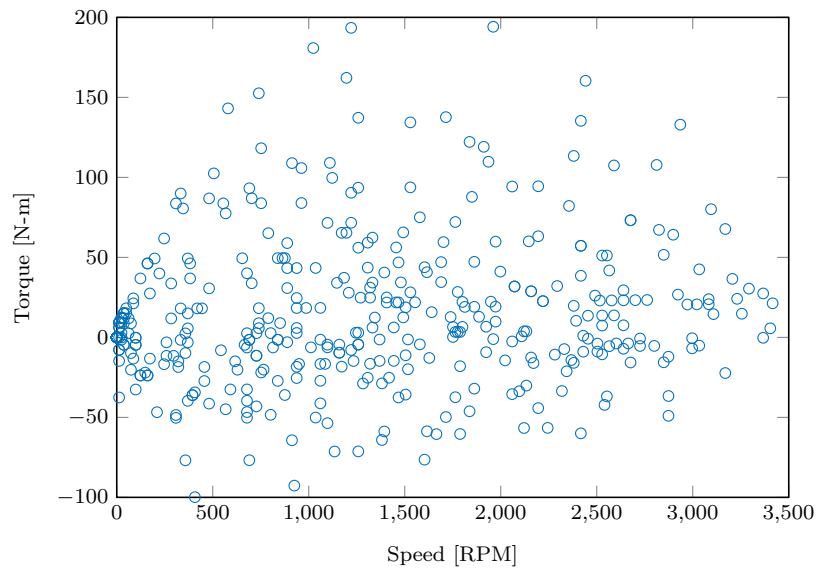


Figure 2.12: Operating Points of EV motor for NYCC cycle

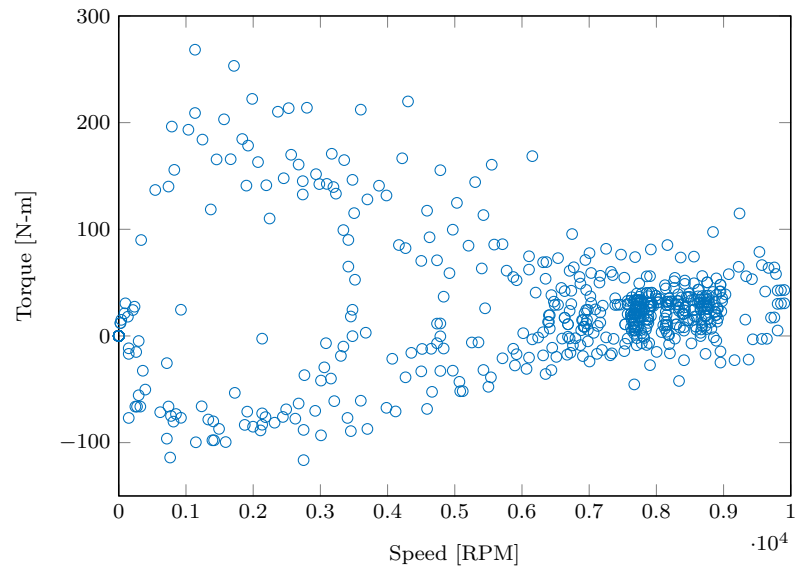


Figure 2.13: Operating Points of EV motor for US06 Cycle

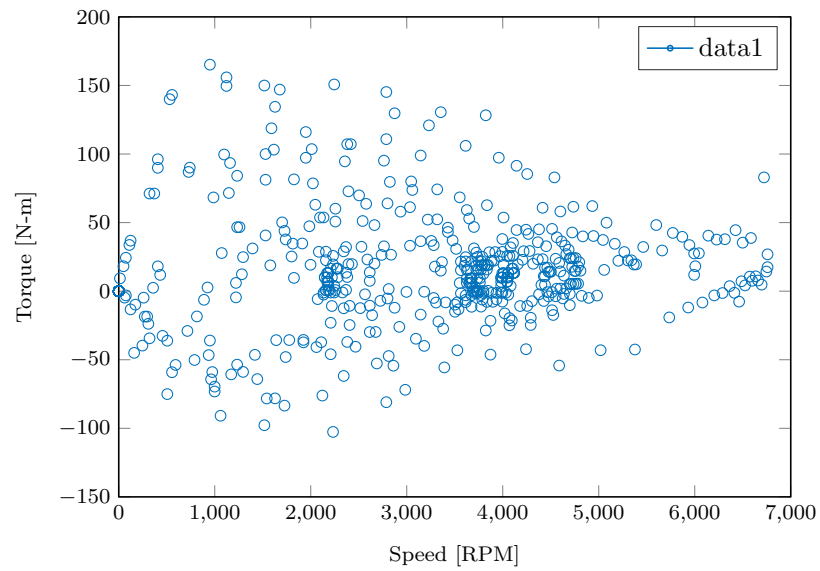
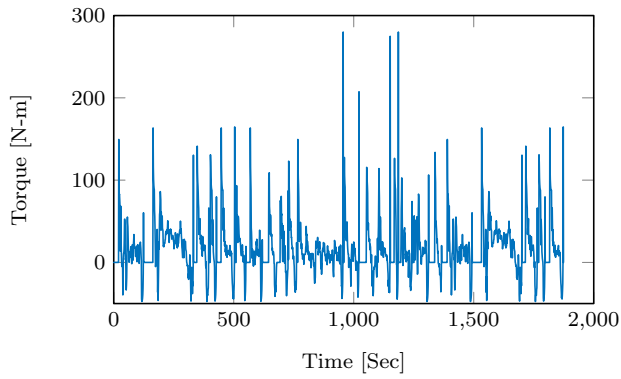
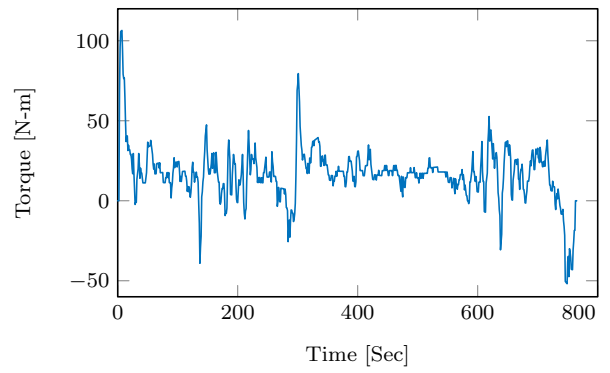


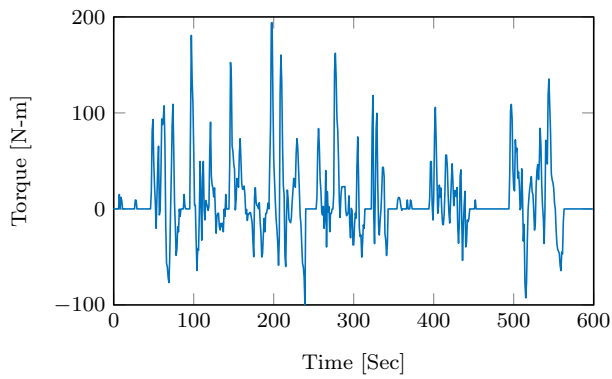
Figure 2.14: Operating Points of EV motor for SC03 Cycle



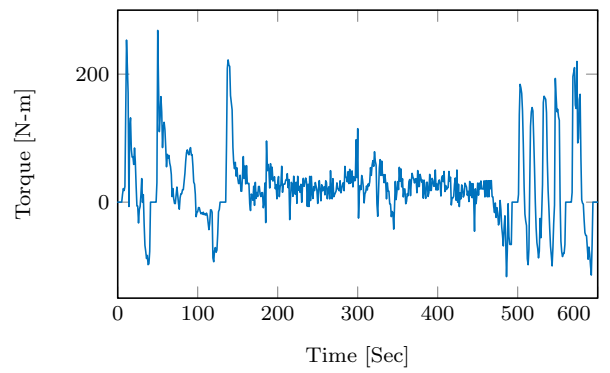
(a) Torque for city Cycle



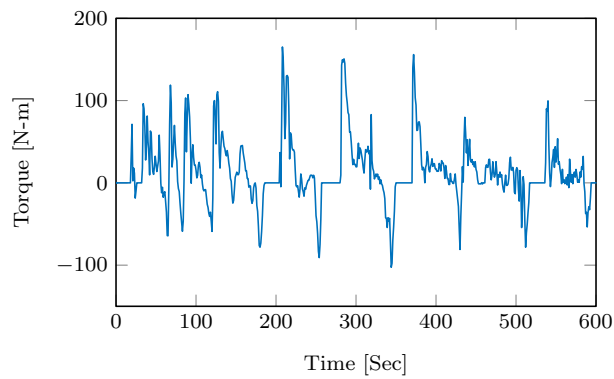
(b) Torque for highway cycle



(c) Torque for NYCC cycle



(d) Torque for US06 cycle



(e) Torque for SC03 cycle

Figure 2.15: Torque required by EV motor for different driving cycles

## CHAPTER 3

### INVERTER MODELLING

#### 3.1 Introduction

Since 1950s, it was considered that WBG devices will be advantageous and will be next step, since Si has reached its physical limits. SiC MOSFETs have less switching losses than Si IGBT but have higher cost which causes difficulty for large scale adoption of SiC devices. As an example, it took almost 50 years until 2001 to become SiC schottky diode to become commercially available. Along with GaN has also been emerged as promising switching device with small size and low losses.

Important characteristic of power semiconductor device is whether its on-state resistance and forward voltage drop exhibit a positive temperature coefficient [4]. Such devices are advantageous for parallel connection with high current operation. Whenever positive temperature coefficient devices are connected in parallel and if high current flows through one device than its on-state resistance increase due to increase in device temperature which forces current to share equitably among the parallel connected devices. Therefore, parallel connection of such devices is less susceptible for hot spot formation and breakdown problems. But diodes cannot be easily connected parallel since they are negative temperature coefficient devices. Variation in one of the diode characteristics can lead to increase in temperature of diode due to conduction of more current. Therefore, parallel connection of any semiconductor devices depends upon many factors like external circuitry, devices characterization matching, heat sink which are essential to cause the on-state currents of the device to be shared equally [4].

For high power switching converters, IGBT devices are more advantageous than MOSFETs mainly due to two factors. One is lower conduction loss and other is lower cost of device, but IGBT have higher switching loss than MOSFETs specifically due to the high

tail current during turn off duration because of which IGBT use is restricted for higher switching frequency [14].

## 3.2 Overview of Switching Devices

The EV inverter losses (such switching loss and conduction loss) calculation is important for evaluating the overall efficiency of the system. In this section, inverter loss modelling with brief explanation of different switching devices such as MOSFET, IGBT which can be used in inverter are discussed along with the switching behaviour in the following section.

### 3.2.1 MOSFET (Metal Oxide semiconductor Field effect transistor)

MOSFET is voltage-controlled switching device and its cross section is shown in Fig. 3.1. As shown in Fig 3.1, the  $n^-$  region is lightly doped for obtaining the desired breakdown voltage. The on-state resistance of device is sum of  $n^-$  region, channel, the source and drain contacts. Therefore, as breakdown voltage increases, the on-state resistance also increases and also, due to absence of minority carriers, conductivity modulation does not take place which increases resistance rapidly as breakdown voltage increase [4]. The symbol of power MOSFET with the parasitic capacitance is shown in Fig. 3.2.

On-state resistance of MOSFET is function of breakdown voltage is expressed as shown in equation 3.1 [14],

$$R_{ds(on)} = k \cdot BV_{DSS}^{(2.5-2.7)} \quad (3.1)$$

Where,

$k$  = constant that depends upon the device geometry

$BV_{DSS}$  = Blocking voltage rating

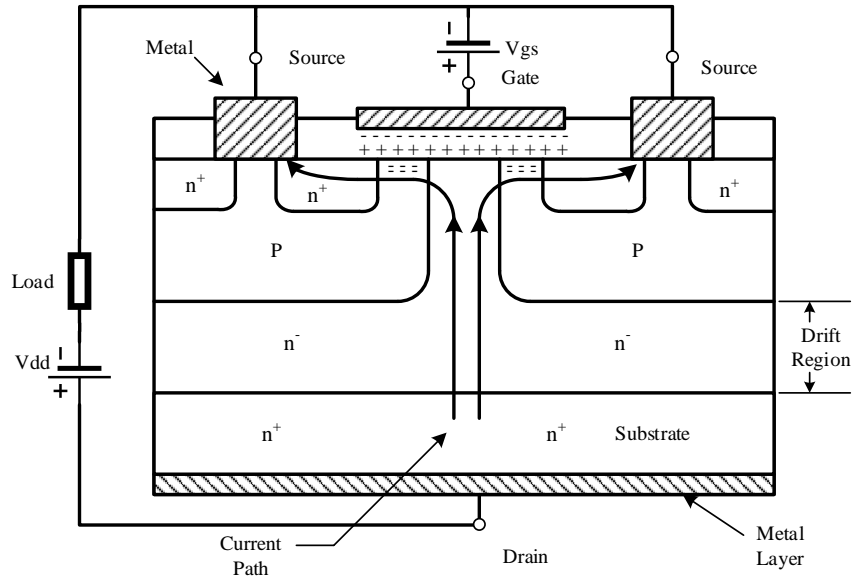


Figure 3.1: Power MOSFET structural view

Therefore, MOSFET with low voltage rating are available which have low on state resistance resulting in small conduction loss. Their switching time is very short, in the range of few tens of nanosecond to few hundred nanoseconds thus they are capable of switching at higher frequencies. It also contains p-n junction body diode which conducts when  $V_{ds}$  is negatively biased. This body diode is not optimized with respect to the speed of the MOSFET, therefore large peak currents can cause the device failure. Hence fast recovery body diodes with peak current handling capacity is provided.

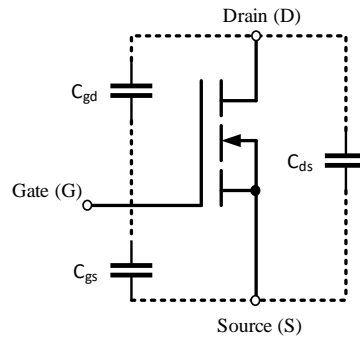


Figure 3.2: MOSFET symbol considering the parasitic capacitance's present in MOSFET [14]

Appropriate magnitude of gate voltage is required for MOSFET to remain on and no gate current flows except during transition. The rate at which drain current changes depends on the rate at which gate to drain capacitance charged. The drain to source capacitance leads directly to switching loss. The gate to source capacitance is basically linear but gate to drain and drain to source capacitance are non-linear and depends on the construction of device. Unlike other power devices, MOSFETs are selected on basis of on-state resistance and not on rated average current. They are preferred for voltage range of 400-500V. Whenever voltages are greater than 400-500V, devices with minority carriers are preferred such as IGBT, which will have low forward voltage drop due to conductivity modulation.

### 3.2.2 MOSFET Switching waveform

The turn on and turn off waveforms of MOSFET with ideal free-wheeling diode are shown in Fig. 3.3 and 3.4 respectively. After gate pulse is given, during turn on delay  $t_{d(on)}$  the gate source voltage  $V_{GS}$  rises almost linearly from zero to  $v_{GS(th)}$  with time constant  $\tau_1 = R_G \cdot (C_{gs} + C_{gd1})$  where ( $C_{gs}$  and  $C_{gd1}$ ) are gate source and gate drain capacitance respectively. Beyond  $V_{GS(th)}$ ,  $V_{GS}$  rises linearly as before, and drain current begins to increase. The time required for drain current ( $i_D$ ) to rise from zero to full load current ( $I_o$ ) is rise time  $t_{ri}$ . Till rise time is reached drain- source voltage ( $V_d$ ) is constant. Once MOSFET is carrying  $I_o$  but is still in active region, gate-source voltage  $v_{GS}$  becomes temporarily clamped to  $V_{GS,I_o}$  to maintain drain current at  $I_o$ . Then entire gate current flows through  $C_{gd}$  which causes  $V_{DS}$  to drop. The drop in  $V_{DS}$  occurs in two time intervals  $t_{fv1}$  and  $t_{fv2}$  as shown in Fig. 3.3.  $t_{fv1}$  corresponds to active region when  $C_{gd} = C_{gd1}$  and  $t_{fv2}$  corresponds to completion of transient in ohmic region where  $C_{gd} = C_{gd2}$ . Once the  $V_{DS}$  reaches to its on-state value  $I_o \cdot r_{DS(on)}$ , the  $V_{GS}$  rises exponentially to  $V_{GG}$  with time constant of  $\tau_2 = R_G \cdot (C_{gs} + C_{gd2})$  and simultaneously gate current decays to zero.

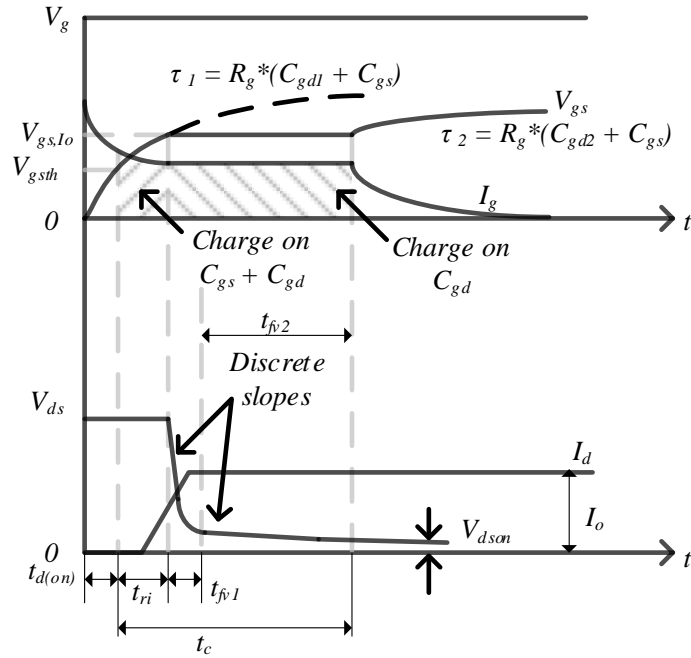


Figure 3.3: MOSFET turn on switching waveform considering ideal free wheeling diode [14]

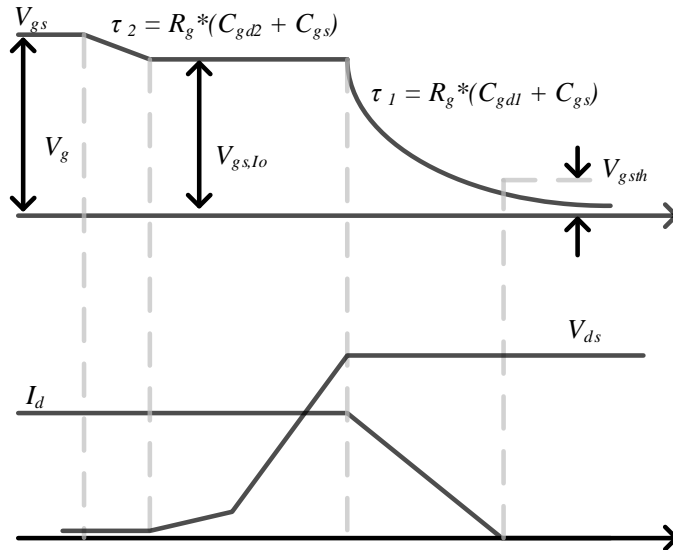


Figure 3.4: MOSFET turn off switching waveform considering ideal free wheeling diode [14]

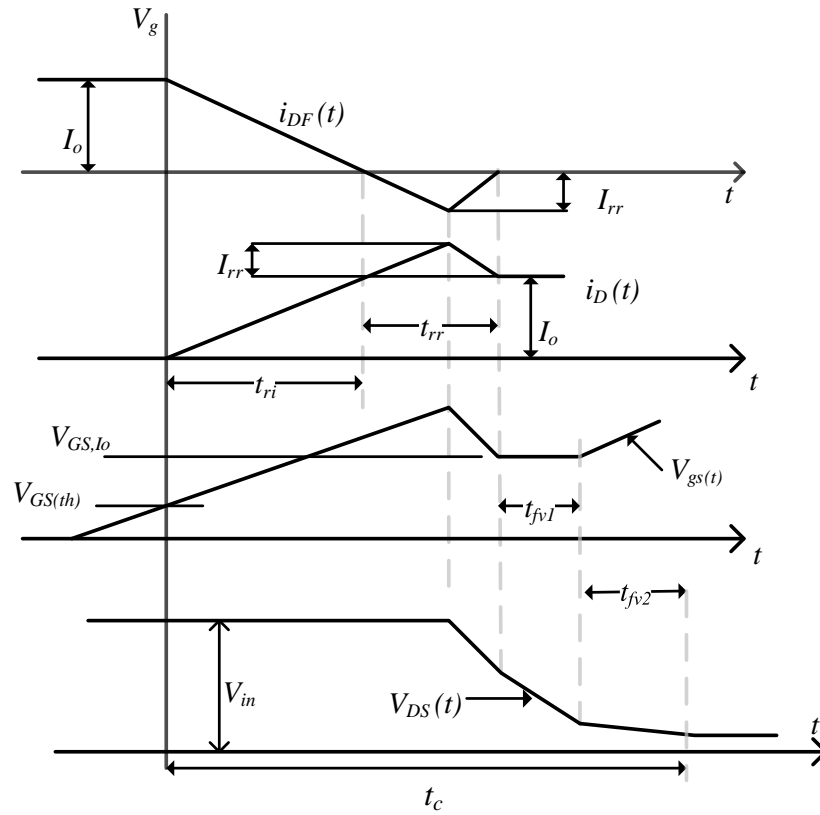


Figure 3.5: MOSFET switching waveform with non-ideal free wheeling diode [14].

If the free-wheeling diode is not ideal then modified switching wave-forms are shown in Fig. 3.5 . During current rise, the drain current rises beyond  $I_o$  to  $I_o + I_{rr}$  which also increases  $V_{GS}$  above its nominal value. When diode current recovers to zero then  $v_{GS}$  decreases to  $v_{GS,I_o}$ . The additional current causes  $V_{DG}$  and  $V_{DS}$  to decrease rapidly. The turn off of MOSFET involves inverse sequence of events as that of turn-on. Since the MOSFET capacitance do not vary with junction temperature, therefore power loss occurred during turn on and turn off is independent of junction temperature [22], [3], [14].

Advantages and Disadvantages of SiC-MOSFET based inverter:

- Development of wide band gap devices such as SiC MOSFET, has cultivated great attention of manufactures and researchers due to its inherent material advantages over Si IGBT [23].
- Due to high saturation velocity of free charges resulting in less time for recombination, which significantly reduces the switching losses of inverter. [9].
- SiC base inverter can operate at higher junction temperature and it is reliable over wide range of temperature range [9].
- The cost of SiC based inverter will be very high compared to Si IGBT based inverter.

### 3.2.3 IGBT (Insulated Gate bipolar transistor)

As shown in Fig. 3.6, the construction of IGBT is much similar to MOSFET. The notable difference is that, P region is connected to IGBT collector instead of N region as seen in MOSFET. The main function of P region is to inject minority charges into N region which causes conductivity modulation. Presence of conductivity modulation, on-state resistance of IGBT reduces enabling manufacturing of high voltage device (as high as 4500V) with low forward voltage drop (2 to 4V), but IGBT has high switching loss compared to MOSFET caused due to current tailing during turn off instants.

From Fig. 3.6, it can be seen that there are two currents flowing through IGBT : the effective MOSFET channel current and PNP collector current. Suppose negative voltage is applied across the gate - emitter junction then, effective MOSFET channel current can be reduced to zero by removing the gate charge. Removal of charges in N region cannot be done actively and PNP collector current decays slowly causing current tail. This tail current can be reduced, but then on-state resistance of IGBT increases. The turn off energy of IGBT is significantly high compared to MOSFET (in range of 0.5 $\mu$ s to 5 $\mu$ s). IGBT can not

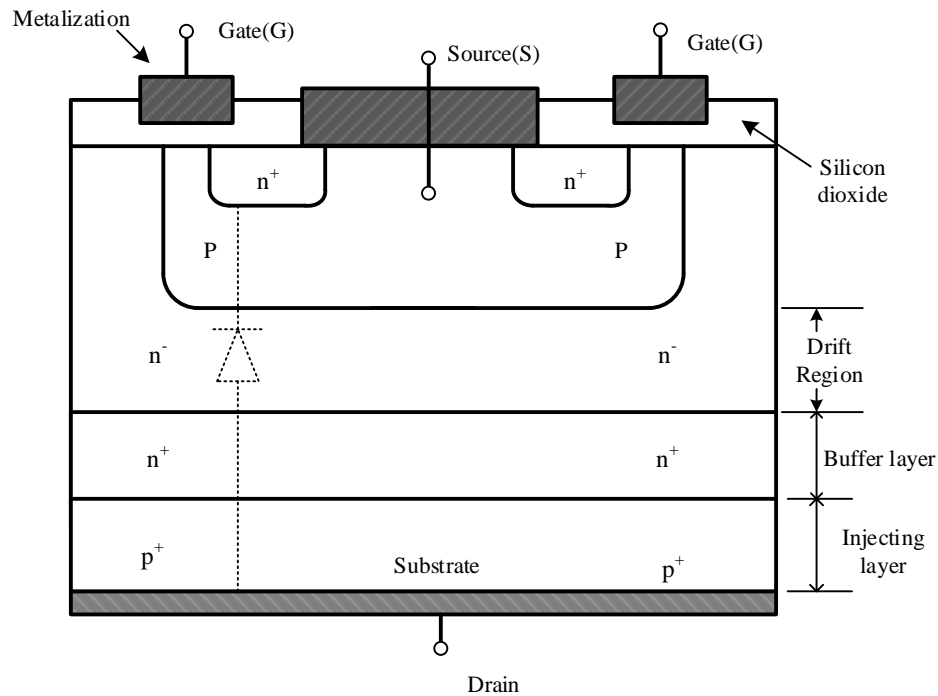


Figure 3.6: IGBT structure [14]

block the reverse voltage since the P-N(-) junction is not capable of handling reverse voltage. Due to the conductivity modulation, the IGBT is popular for easy connection in parallel operation. Many modules are commercially available with multiple parallel connecting chips [4].

### 3.2.4 IGBT switching waveform

The current and voltage waveform for corresponding turn on and turn off are shown in Fig. 3.7 and 3.8. The turn on portions for IGBT looks similar to that of MOSFET since IGBT essentially act as MOSFET during most of the turn on interval. The interval  $t_{fv2}$  in IGBT is contributed due to two factors. First, the gate-drain capacitance  $C_{gd}$  increases at low drain-source voltages similar to that of MOSFET and second PNP transistor portion of IGBT transverses the active region to its on state more slowly than MOSFET portion

of IGBT. Until the PNP transistor is full on, the benefit of conductivity modulation in drain-drift region is not achieved, and therefore the voltage drop across the IGBT has not dropped to its final value.

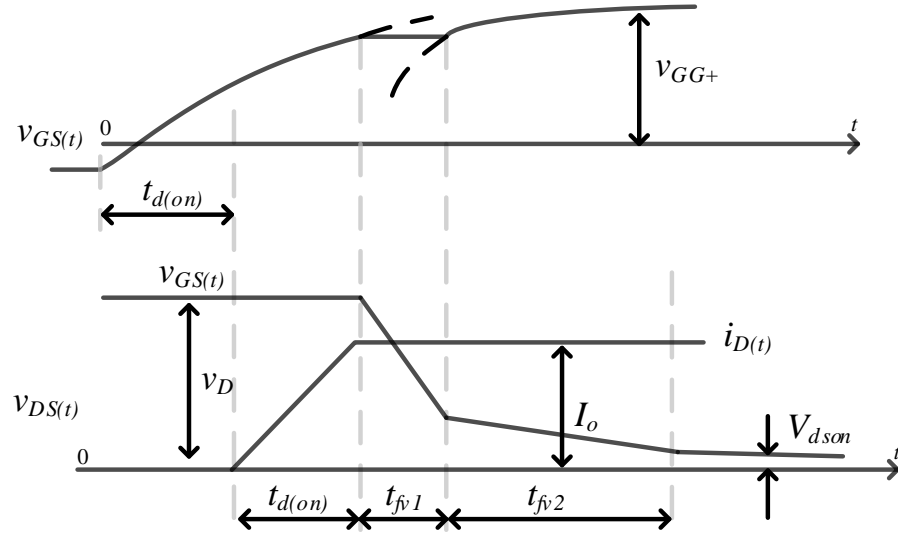


Figure 3.7: Detailed explanation for IGBT turn on process [14]

During turn off transient, the turn off delay  $t_{d(off)}$ , voltage rise time  $t_{rv}$  is due to the MOSFET portion of IGBT. The rapid drop in drain current during  $t_{fv1}$  is due to MOSFET section present in IGBT while the tailing of drain current in interval  $t_{fv2}$  is due to stored charges in  $n^-$  drift region. The excess carrier lifetime is desirable for low voltage drop, but then the duration for turn off increases and even power dissipation in this interval will increase which is undesirable. This time increases with temperature and hence tailing time increases. Thus, the trade off between on state loss and faster turn off times must be made in IGBT. Punch-through IGBT minimizes the current tailing problems by adding  $n^+$  buffer layer, while non punch through IGBTs attack current tailing by minimizing the magnitude

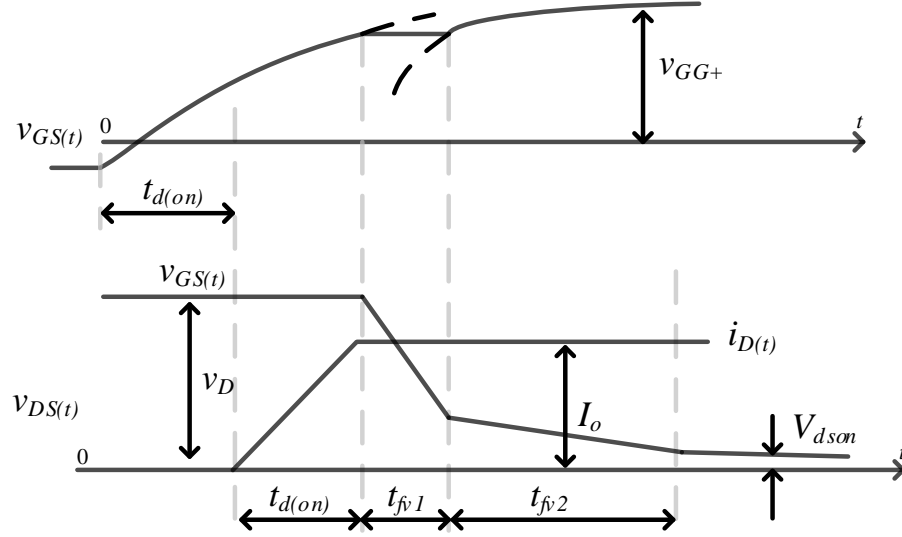


Figure 3.8: Detailed explanation for IGBT turn off process [14]

of current during tailing period. The comparison between Si, SiC and GaN in terms of material properties is provided in Table 3.1.

Table 3.1: Material Properties of silicon, GaN and SiC [2]

Parameter	Silicon	GaN	SiC
Band Gap ( $eV$ )	1.12	3.39	3.26
Critical Field ( $MV/cm$ )	0.23	3.3	2.2
Electron Mobility ( $cm^2/V \cdot s$ )	1400	1500	950
Permittivity	11.8	9	9.7
Thermal conductivity ( $W/cm \cdot K$ )	1.5	1.3	3.8

### 3.3 Inverter Modelling

The inverter can be designed considering different semiconductor devices (switching device) and every semiconductor device has its own advantages and disadvantages. Use of new

material, new/modified inverter topology or improved control strategy is essential for realizing inverter with improved efficiency.

In this thesis, a typical three phase full bridge inverter with different switching device is considered. The major portion of losses occurs in power electronics block is due to semiconductor devices. The losses in a semiconductor devices can be classified as conduction loss and switching loss. The leakage current during off state is very small and therefore power loss during off state can be neglected in practice [15], [21].

Different techniques are developed in scientific literature for calculating power electronic converter losses [11]. The most simple model for determining the losses is by considering power converter as equivalent resistive load, where inner power losses are proportional to square of current flowing through the converter. Hence, power loss expression can be formalized using equation 3.2, where  $R_{Inv}$  is inverter equivalent resistance and  $I$  is Root Mean Square (RMS) of inverter output phase current which is equivalent to electric motor input phase RMS current [11], [13], .

$$P_{LossInv} = 3 \cdot R_{Inv} \cdot I^2 \quad (3.2)$$

The inverter input power can be calculated by adding inverter losses  $P_{LossInv}$  to input motor power  $P_{InMot}$  which is same as  $P_{OutInv}$

$$P_{InInv} = P_{LossInv} + P_{InMot} = P_{LossInv} + P_{OutInv} \quad (3.3)$$

The more detailed inverter loss model for IGBT and MOSFET is discussed in this section. The losses are computed considering basic inverter cell. The analytical technique is used to calculate the device losses in PWM inverter considering the symmetrical double edge sinusoidal modulation, assuming sinusoidal load current. Bessel function solution is used to reduce loss equation to simple algebraic equation [13]. The instantaneous losses of IGBT basic cell is calculated using equation 3.4

$$\left\{ \begin{array}{l} pfwT = v_{ce}(i_c) \cdot i_c \\ pfwD = v_{ak}(i_f) \cdot i_f \\ pswT = [E_{on}(i_c) + E_{off}(i_c)] \cdot f_s \\ p_{recD} = E_{recD}(id) \cdot f_s \\ p_{cell} = p_{swT} + p_{recD} + pfwT + pfwD \end{array} \right\} \quad (3.4)$$

Where,  $v_{ce}$  = IGBT forward voltage drop,  $v_{ak}$  = Diode forward voltage drop,  $i_c$  = IGBT direct current,  $i_f$  = Diode direct current,  $f_s$  = Inverter switching loss,  $E_{on}$  = IGBT turn on energy,  $E_{off}$  = IGBT turn off energy,  $E_{recD}$  = Diode recovery energy,  $pfwT$  = IGBT conduction forward losses,  $pfwD$  = Diode conduction forward losses,  $p_{recD}$  = Diode power losses,  $p_{swT}$  = IGBT switching losses,  $p_{cell}$  = Loss for one IGBT cell.

Total losses in inverter, can be calculated using equation 3.5

$$P_{inv} = 6 \cdot p_{cell} \quad (3.5)$$

The IGBT and diode typical forward characteristics (current vs voltage) and switching on and off energies can be obtained from the switch data sheet or can be evaluated experimentally. The curve fitting tool from MATAB is used to get the curve fitted equation for the forward characteristics and switching energy characteristics, from which the required constants for equation 3.6 are found to acquire the voltage relationship in terms of current flowing through switch.

$$\left\{ \begin{array}{l} v_{ce}(i_c) = A_{fwT} + B_{fwT}i_c \\ v_{ak}(i_f) = A_{fwD} + B_{fwD}i_f \\ E_{on}(i_c) = B_{on}i_c + C_{on}i_c^2 \\ E_{off}(i_c) = B_{off}i_c + C_{off}i_c^2 \\ E_{recD}(i_f) = B_{recD}i_f + C_{recD}i_f^2 \end{array} \right\} \quad (3.6)$$

Substituting the equation 3.6 into equation 3.4, we get equation 3.7. These equations express instantaneous power loss of IGBT based inverter in terms of it's current.

$$\left\{ \begin{array}{l} p_{fwT}(i_c) = A_{fwT}(i_c) + B_{fwT}i_c^2 \\ p_{fwD}(i_f) = A_{fwD}(i_f) + B_{fwD}i_f^2 \\ p_{swT}(i_c) = (B_{on}i_c + C_{on}i_c^2)f_s + (B_{offT}i_c + C_{offT}i_c^2)f_s \\ p_{recD}(i_f) = (B_{recD}i_f + C_{recD}i_f^2)f_s \end{array} \right\} \quad (3.7)$$

For calculating the inverter loss, instantaneous three-phase motor current needs to be calculated, for which the simulation time step should be very short considering high computational load. For EV modelling, such accuracy is not required, but exact loss calculation is important for substantially large time duration. An average approach is considered which is sufficient for EV modelling with power flow analysis.

$$\left\{ \begin{array}{l} P_{fwT} = \left(\frac{1}{2} - \frac{T_{dead}}{T_s}\right) \left(\frac{A_{fwT}}{\pi} I_M + \frac{B_{fwT}}{4} I_M^2\right) + m \cdot \cos(\phi) \left(\frac{A_{fwT}}{8} I_M + \frac{B_{fwT}}{3\pi} I_M^2\right) \\ P_{fwD} = \left(\frac{1}{2} - \frac{T_{dead}}{T_s}\right) \left(\frac{A_{fwD}}{\pi} I_M + \frac{B_{fwD}}{4} I_M^2\right) + m \cdot \cos(\phi) \left(\frac{A_{fwD}}{8} I_M + \frac{B_{fwD}}{3\pi} I_M^2\right) \\ P_{onT} = f_s \cdot I_M \left(\frac{B_{onT}}{\pi} + \frac{C_{onT}}{4} I_M\right) \\ P_{offT} = f_s \cdot I_M \left(\frac{B_{offT}}{\pi} + \frac{C_{offT}}{4} I_M\right) \\ P_{recD} = f_s \cdot I_M \left(\frac{B_{recD}}{\pi} + \frac{C_{recD}}{4} I_M\right) \\ P_{PWM} = P_{onT} + P_{offT} + P_{fwT} + P_{fwD} + P_{recD} \end{array} \right\} \quad (3.8)$$

Where,  $I_M$  is peak value of fundamental phase current (assuming sinusoidal time dependency for current),  $\omega = 2\pi/T$  is angular current frequency,  $T_s$  is IGBT switching period,  $T_{dead}$  is dead time between high and low side of IGBT in phase leg configuration,  $\cos(\phi)$  is motor power factor,  $P_{invPWM}$  is total averaged inverter losses. The total inverter loss can be calculated by substituting the values found in equation 3.8 in equation 3.9.

$$P_{invPWM} = 6 \cdot P_{PWM} \quad (3.9)$$

Similar to IGBT, the loss calculation for MOSFET in an inverter can also be modelled [20]. The forward characteristics is linearized and voltage  $v_{ds}$  can be modelled as function of switch current  $i_{ds}$  with constant voltage drop  $V_{ds,0}$  and resistance  $R_{ds,on}$  using curve fitting tool from MATLAB. The forward voltage drop is represented in equation 3.10,

$$v_{ds} = V_{ds,0} + R_{ds,on} i_{ds} \quad (3.10)$$

The inverter conduction loss is however dependent on the power factor ( $\phi$ ) and modulation index ( $m_a$ ). The conduction loss for a MOSFET switch and diode in an inverter is expressed as shown in equation 3.11

$$P_{fw,mosfet} = V_{ds,0}I_M\left(\frac{1}{2\pi} + \frac{1}{8} \cdot m_a \cos(\phi)\right) + R_{ds,on}I_m^2\left(\frac{1}{8} + \frac{m_a}{3\pi} \cos(\phi)\right) \quad (3.11)$$

where,  $I_M$  is the peak value for the fundamental of phase current. Similar to MOSFET the conduction loss can be modelled for diode considering diode current  $i_f$ , diode voltage  $v_f$  and  $V_{f,0}$  constant voltage drop as follows:

$$v_f = V_{f,0} + R_{f,on}i_f \quad (3.12)$$

$$P_{fw,diode} = V_{f,0}I_M\left(\frac{1}{2\pi} + \frac{1}{8} \cdot m_a \cos(\phi)\right) + R_{f,on}I_m^2\left(\frac{1}{8} + \frac{m_a}{3\pi} \cos(\phi)\right) \quad (3.13)$$

Switching losses of MOSFET can be modelled as [10]

$$P_{sw,mosfet} = (V_{DS}I_D t_{on,M} + V_{DS}I_D t_{off,M}) \cdot f_s \quad (3.14)$$

where,  $t_{on,M}$  and  $t_{off,M}$  are the turn on and turn off times of the MOSFET, respectively.  $V_{DS}$  and  $I_D$  are voltage across MOSFET and current through it at time of commutation, respectively. The switching losses of diode considering the reverse recovery losses  $Q_{rr}$  and battery voltage  $V_{Batt}$  can be given as,

$$P_{sw,D} = (Q_{rr}V_{Batt})f_s \quad (3.15)$$

The total average loss for one MOSFET cell is summation of the switching and conduction losses for switch and diode, which is given as

$$P_{PWM} = P_{fw,mosfet} + P_{fw,diode} + P_{sw,mosfet} + P_{sw,D} \quad (3.16)$$

and the total averaged inverter losses  $P_{invPWM}$  is given as

$$P_{invPWM} = 6 \cdot P_{PWM} \quad (3.17)$$

Since the inverter model receives input parameters such as  $V_s$ ,  $I$  and  $\cos(\phi)$  from motor model and assuming the fixed battery voltage  $V_{batt}$  as input parameter, the current required to the battery  $i_{inv}$  and total inverter losses can be calculated using following set of equations:

1. Total Power supplied to the motor calculation :  $P_{InMot} = \sqrt{3} \cdot V_s I \cos(\phi)$ ,
2. Inverter AC phase current max. value calculation :  $I_M = \sqrt{2} \cdot I$
3. Inverter PWM amplitude modulation index calculation :  $m = \sqrt{2} V_s / V_{batt}$
4. total inverter averaged losses  $P_{invPWM}$  calculation by means of equation 3.9 and 3.17.
5. Total inverter power calculation :  $P_{InInv} = P_{InMot} + P_{invPWM}$
6. Inverter input current calculation :  $i_{inv} = P_{InInv} / V_{batt}$

## CHAPTER 4

### AUXILIARY INVERTER CONFIGURATION

For high power switching converters, IGBT devices are more advantageous than MOSFETs mainly because of two factors. One is lower conduction loss and other lower cost, but IGBTs have higher switching loss than MOSFETs specifically due to the high tail current during turn off duration because of which IGBT use is restricted for higher switching frequency. Using WBG devices i.e., SiC MOSFET and GaN switch higher switching frequencies can be achieved, but the overall cost of the system increases.

EV inverters are designed with peak power rating. Therefore, as power handling capacity of inverter increases, size, heat dissipation and power losses of inverter also increases. No system gives high power and performance at a time with high reliability and easy maintainability, therefore these inverters have low efficiency at light load conditions and inverter with WBG devices elevates the cost which is not desirable [8]. Thus auxiliary inverter configuration in parallel to main inverter can be used during low load current requirement and to assist the main inverter for switching during high power requirement. This will help to achieve cost effective and efficient EV inverter.

#### 4.1 Double Pulse Test

The LT-SPICE simulation is carried out to find the switching loss for GaN device. The Fig. 4.1 shows the schematic for double pulse test of (GS66508T) GaN device. The double pulse test is mainly carried out to analyze the switching characteristics and behaviour of device. It uses purely inductive load and observes switching behavior without heating the switching devices. Even the rising edge and falling edge of switches are analyzed.

As shown in figure, L5 and L6 are the gate resistances, L7 and L9 are the external source inductances, L1 is the load inductor, L11 and L14 are considered as power loop inductances.

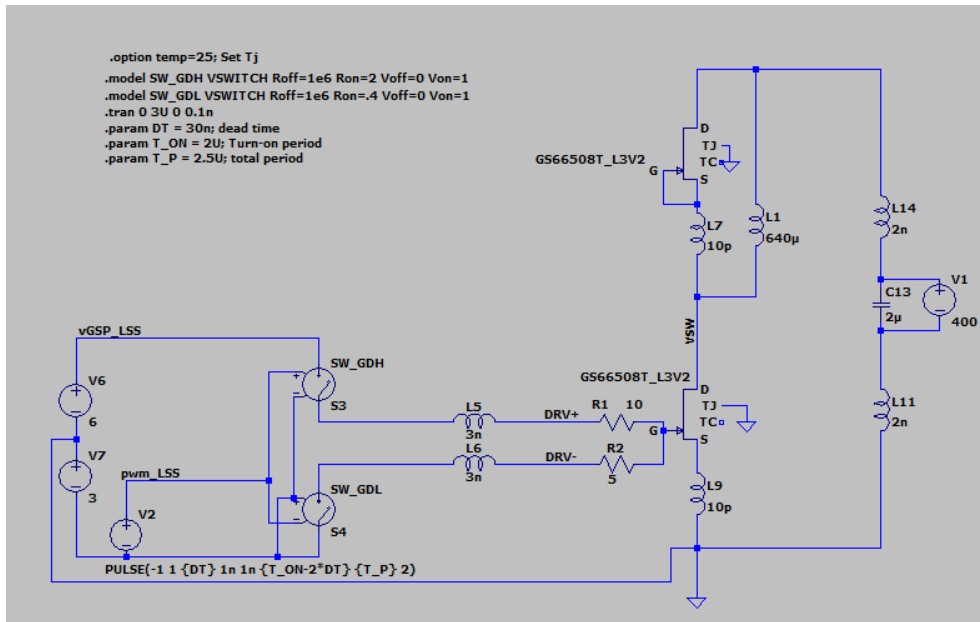


Figure 4.1: Double Pulse test for GaN switch for power loss calculation

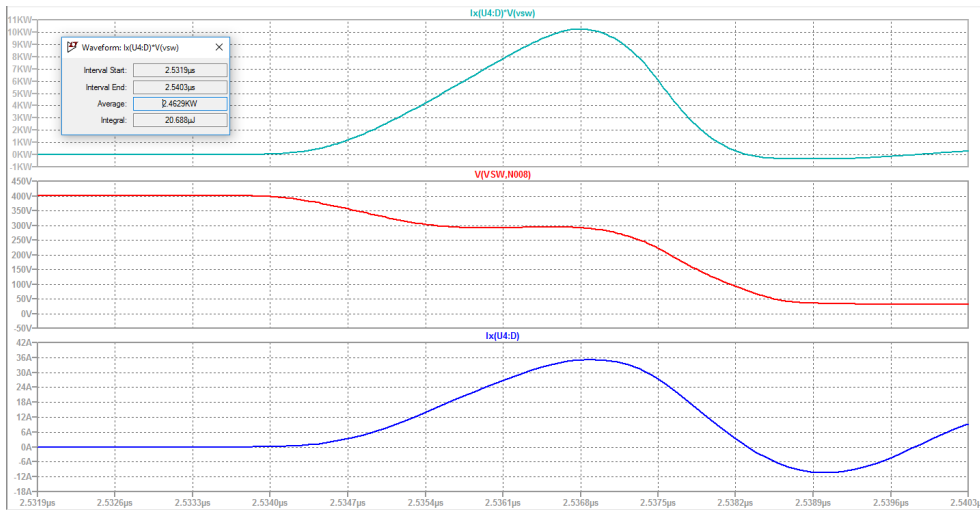


Figure 4.2: Double Pulse test for GaN switch for turn on loss

After the simulation, the turn on and turn off energies are computed and it is found that turn on power loss is about  $20.7 \mu\text{J}$ , while the turn off loss is about  $7.3 \mu\text{J}$  as shown in Fig.

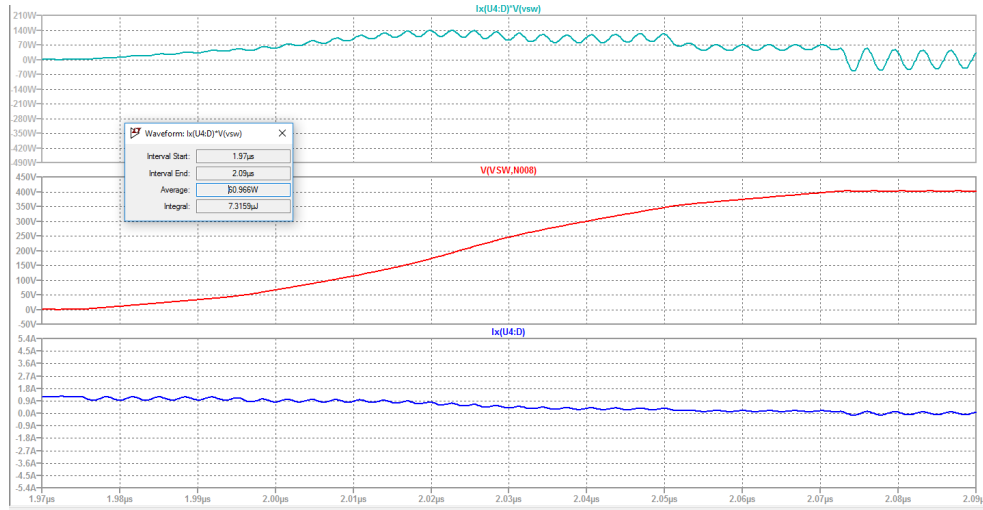


Figure 4.3: Double Pulse test for GaN switch for power loss calculation

4.2 and 4.3. The energy loss found from simulation is used for thermal modeling in PLECS software for loss calculation and inverter efficiency calculation.

## 4.2 Description of auxiliary inverter configuration

High efficiency at light load condition with high power handling capacity can be supported with parallel combination of two inverters. The basic idea in this thesis is to use two converters in parallel with each other in such a way that one inverter can handle full rated power required by load and the other inverter (auxiliary inverter) can be used at light load condition or to assist the main inverter at time of high-power requirement. Auxiliary inverter is modelled such that it can handle some fraction of rated power. The switching device used in main inverter is Si IGBT (device with lower conduction loss) and the auxiliary inverter consists of WBG device (device with low switching loss). Low conduction loss of Si IGBT and low switching loss of WBG devices i.e. SiC MOSFET / GaN is very advantageous for paralleling of inverter. Implementation of inverter is done in such a way that conduction loss is taken care by Si-IGBT based inverter i.e. main inverter and switching loss is taken

care by WBG device (SiC MOSFET / GaN) based inverter i.e. auxiliary inverter. The block diagram explaining the configuration of auxiliary inverter configuration is shown in Fig. 4.4

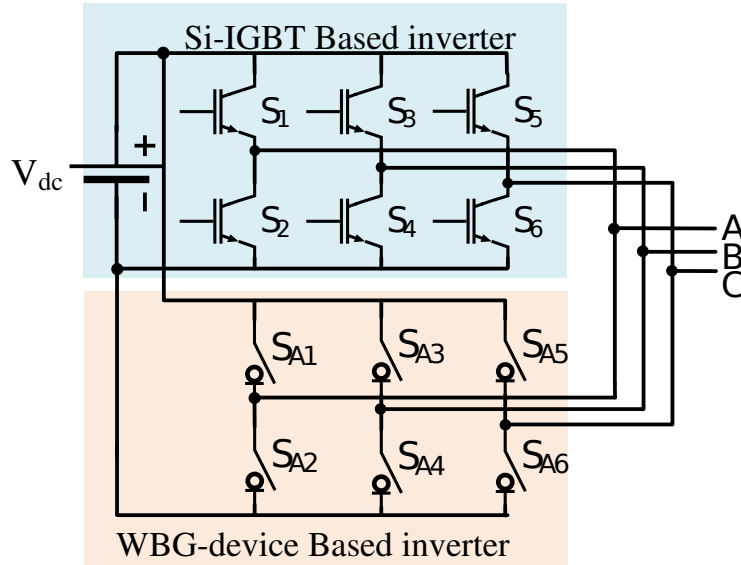


Figure 4.4: Block diagram of auxiliary WBG based inverter with Si based main inverter.

### 4.3 Gate control strategy

The gate control strategy used for auxiliary inverter configuration is explained in this sections. This configuration takes the advantage of good conduction characteristics of the Si-IGBTs and good switching characteristics of WBG devices. The auxiliary inverter assists the main converter during turn on and turn off duration, eliminating the high switching loss issues of Si-IGBTs.

Consider the load requirement of EV is divided into three categories: low, medium and high power. This categorization is mainly a function of power handling capacity of auxiliary inverter and the amount of power required for maximum amount of time over a range by EV. The power handling capacity of inverter is determined from the rating of

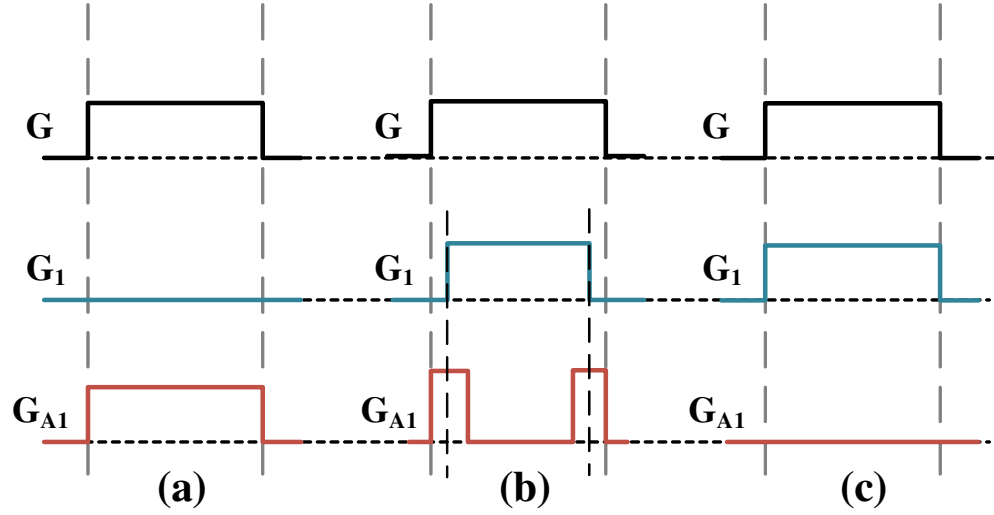


Figure 4.5: Gate control strategy

switching device used. The switching scheme to operate this parallel connected inverter system have three different modes. Fig. 4.5 presents the gate pulses to be applied during different modes of operation. In which, suppose  $G$  is the gate pulse that need to be applied to conventional inverter then  $G_1$  and  $G_{A1}$  represents the gate pulses to Si and WBG based inverter respectively. WBG device rating decision is taken such that optimal energy efficiency is achieved with optimal cost of the system.

The mode of operation are discussed below:

- Mode 1: During this mode of operation, only the auxiliary inverter functions, whereas the main converter remains in off state. This mode would be advantageous during the light load conditions when the load current is small compared to rated load current. This is because, at lower currents, conduction losses offered by the WBG devices would also be small. The boundary condition of this mode depends on the WBG device's continuous current rating. The switching pulses corresponding to both main and auxiliary inverters are shown in Fig. 4.5(a).
- Mode 2: During this operating mode, the WBG device based auxiliary inverter assists the main inverter. This mode of operation is used when the load current is less than

pulsed current rating of WBG devices and greater than the continuous current rating of WBG. The typical ratio of pulse current rating and continuous current rating of WBG devices varies between 2.5 to 3.5. Both the main inverter and auxiliary inverter operates and the gate pulses for the same are shown in Fig. 4.5(b). The WBG device assisted switching of Si-IGBTs ensure very small switching losses. Moreover, the overall system will be energy efficient and cost effective. This is because, if the inverter is modelled using only WBG device with full rated current capacity then even if the losses are low the cost of the system will be high and if the system is modelled with only Si-IGBT then switching losses will increase as load current increases. In the auxiliary inverter system WBG devices are used with the rating which is fraction of the total current rating. The rating of WBG devices can be selected such that the increase in efficiency of inverter is achieved at optimal cost.

- Mode 3: Whenever current through system is higher than the continuous current rating of WBG, only main inverter is operated and auxiliary inverter is disabled. In this mode only Si based main inverter is functional. This mode comes into picture when the load current is larger than the pulse current rating of WBG devices. From Chapter 2, it can be inferred that only for a small duration of time, load current requirement will be high. This mode would result in higher switching losses. But, this is where the trade-off between the efficiency and cost should be considered carefully. This is because choosing the higher rated WBG devices for auxiliary inverter can completely eliminates the requirement of this mode but increases the cost of the system. The gate pulses for Si and WBG devices are shown in Fig. 4.5(c).

#### 4.4 Validation using PLECS software

To evaluate the loss and efficiency distribution in full bridge inverter, first it is simulated in PLECS software with Si IGBT, SiC MOSFET and auxiliary inverter configuration consisting

of GaN and SiC MOSFET as switching device for R-L load. The input voltage assumed to be 400 volts. The IGBT considered for PLECS simulation is IKW30N65NL5 from 'Infineon' manufacturer, SiC MOSFET used is SCT3022AL from 'ROHM' manufacturer and GS66508T as GaN device of 'GaN systems'.

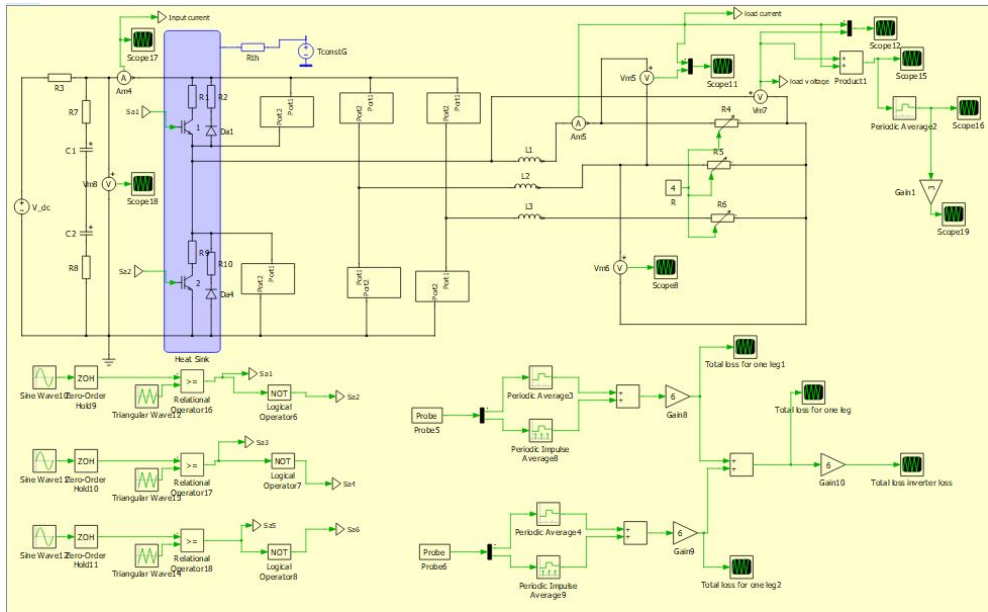


Figure 4.6: Full Bridge inverter loss calculation using PLECS software for only Si IGBT based inverter

The Fig. 4.6 shows the schematic of full bridge inverter used for calculation of losses and inverter efficiency. Sine PWM is used for generating gate pulses for switches. The Si IGBT and SiC MOSFET used are capable of conducting 60A of continuous current. The inverter need to be designed with continuous current of 350 A (considering the NISSAN Leaf inverter maximum current) and therefore six switches are connected in parallel to demonstrate the 350A inverter. Similar to Si IGBT full bridge inverter, efficiency is calculated for SiC MOSFET and also for auxiliary inverter configuration with WBG devices as switching device. The efficiency's obtained for one operating point and are shown in Table 4.1.

As shown in Table 4.1, the efficiency of inverters with different configurations are calculated and compared at one operating point with switching frequency of 20kHz. Using

Table 4.1: PLECS simulation loss comparison considering R-L load for one operating point

<b>Sr. No.</b>	<b>Inverter</b>	<b>Efficiency</b>
1)	Si IGBT based inverter	97.17%
2)	SiC MOSFET based inverter	99%
3)	GaN based inverter	99.3%
3)	Si IGBT(Main inverter) with SiC MOSFET (auxiliary inverter)	98.6%
4)	Si IGBT(Main inverter) with GaN (auxiliary inverter)	98.9%

the modeling discussed in the above Chapters, the energy efficiency of inverter is calculated for city test cycle in MATLAB software. Energy efficiency is efficiency of inverter over a given time range in driving cycle and it is compared as shown in Table 4.2.

Table 4.2: Energy efficiency comparison of different inverter configurations considering city cycle

<b>Sr. No.</b>	<b>Inverter</b>	<b>Energy Efficiency</b>
1)	Si IGBT based inverter	93%
2)	SiC MOSFET based inverter	96.8%
3)	GaN based inverter	97.9 %
4)	Si IGBT(Main inverter) with SiC MOSFET (auxiliary inverter)	97.9%
5)	Si IGBT(Main inverter) with GaN (auxiliary inverter)	98.2%

Table 4.3: Cost of switching devices with almost 60 A continuous current rating which is used in main inverter

<b>Switching Devices</b>	<b>Device number</b>	<b>Cost per switch</b>
Si IGBT	IKW30N65EL5	3.69\$
SiC MOSFET	SCT3022AL	38\$
GaN	GS66516T	55\$

As shown in the Table 4.3, three different devices are compared considering the cost and it can be observed that for 60 A switches the cost of device is high for SiC MOSFET and GaN. If the inverter with 350A peak current rating is considered then with 60A switch current rating, there will be 12 switches per leg are required and for whole inverter 36 switches are required.

Cost of switching device can also be put in terms of cents/ampere i.e. by considering the system current we can calculate the cost required for switching device. From Table 4.3, we can observe that 6.15 cents/ampere is required for IGBT, 63.3 cents/ampere is required for SiC MOSFET and 92 cents/ampere is required for GaN switch.

Referring the Table 4.3, cost of the inverter will increase if we use only WBG devices based inverter. Instead of using GaN for whole inverter if we use auxiliary inverter with fraction of main inverter rating then the cost will be less and as mentioned in above section it can be used at lower load current and to assist main inverter for switching.

#### 4.5 Experimental Verification

The double pulse test schematic and prototype for auxiliary inverter configuration is shown in Fig. 4.7. Prototype is designed in such a way that, it can resemble the a switch from one leg of inverter. As shown in Fig. 4.7, switch  $S_1$  is Si IGBT, switch  $S_{A1}$  is WBG device. The upper diode is used for free wheeling purpose. The Si IGBT is with gate-source terminal connected to each other can be used for free wheeling purpose. The load inductor used is, air core inductor with 640  $\mu$ H value.

As shown in schematic the stray inductance is present in power loop as well as in gate driver loop. If the stray inductances are high than it may catch unwanted noise which can lead to the false triggering of the switch. For GaN device it is very important to have minimum gate as well as power loop inductance and negative voltage must be applied to

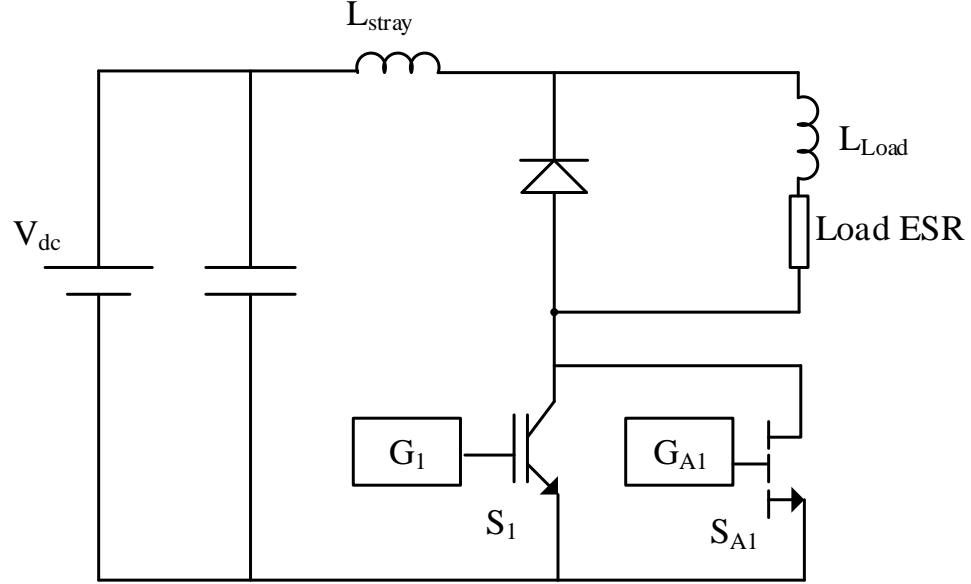


Figure 4.7: Double Pulse test (DPT) prototype. S1 and S2 are Si IGBT and WBG devices respectively,  $V_{dc}$  is DC source

GaN to make sure that GaN switch is turned off, because the noise can also trigger the GaN switch.

The Fig. 4.8 shows the practical prototype used for calculating the energy loss for system. The energy loss is calculated for Si IGBT only using double pulse test. While doing the double pulse test only for GaN switch, noise is observed in measurement. Modification has to be done for GaN side loops to reduce the loop inductances because of which hybrid energy loss has not been calculated yet. Methods are being used to reduce the loop inductance for GaN device. Even while measuring the voltages across different nodes the care should be taken. If the probe used for measuring contains large ground loop than noise has been observed in the measurement, which can be eliminated by use of small ground loop measuring probe.

At different loading conditions i.e. changing the pulse width in double pulse test, different currents through the switch is achieved. Turn on and turn off energies are calculated for Si IGBT are shown in Table 4.4. The switching waveform shown in Fig. 4.9 to 4.12 which are

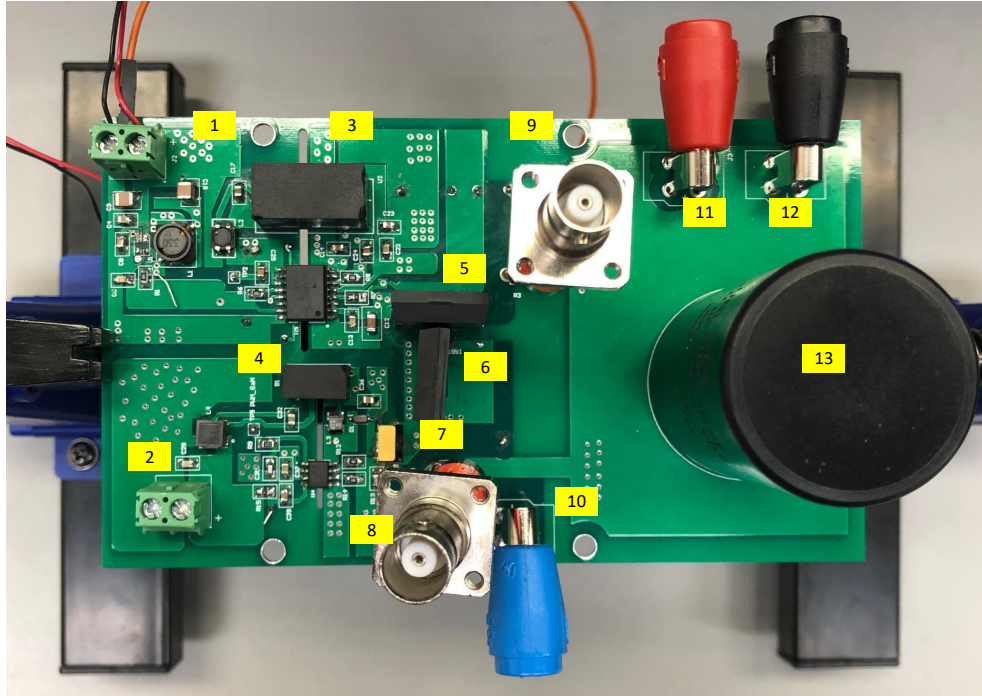


Figure 4.8: Double Pulse test (DPT) prototype. 1. and 2. 12 volts and 5 volts power supply respectively, 3. Isolated DC-DC converter for 12 volts to 15/-5 volts supply, 4. Isolated DC-DC converter for 5 volts to 9 volts supply, 5. Top IGBT switch, 6. Bottom IGBT switch, 7. GaN switch, 8. shunt resistor for current measurement through GaN switch, 9. shunt resistor for current measurement through IGBT switch, 11 and 12. positive and negative DC bus supply, 13. DC link capacitor

Table 4.4: Turn On and turn OFF energy for IGBT at different loading condition considering 640  $\mu\text{H}$  inductor and 400 V input DC supply

Current	Turn Off energy	Turn On energy
10 A	520 $\mu\text{J}$	752.76 $\mu\text{J}$
20 A	641 $\mu\text{J}$	802 $\mu\text{J}$
30 A	954 $\mu\text{J}$	1.13mJ

obtained at 30A of operating condition which shows the drain voltage and switch current. Similarly at different drain current, different energies are calculated. Fig. 4.13 and 4.14 shows the waveform for 50A inductor current, where, green colour waveform is drain source

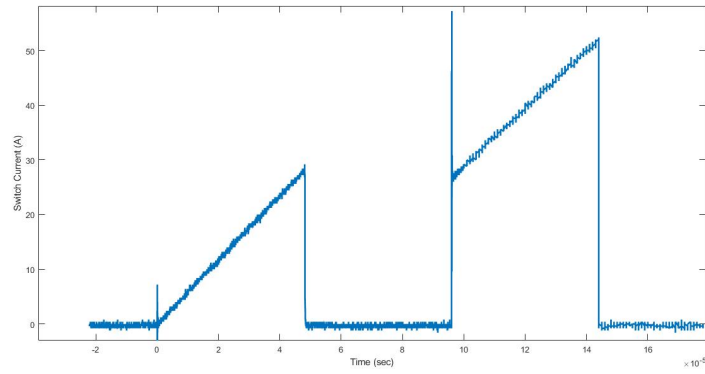


Figure 4.9: Drain Current with turn on period of 48  $\mu$  S

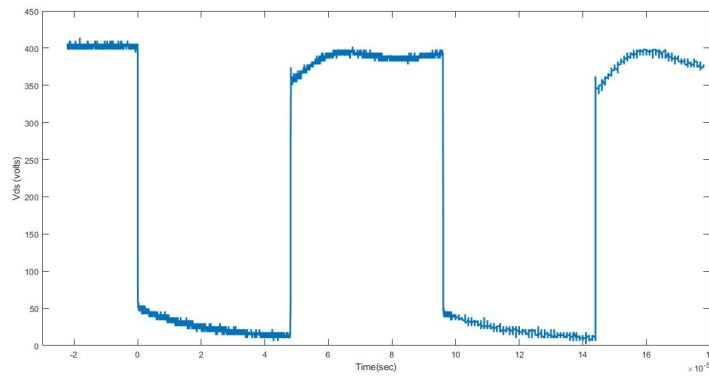


Figure 4.10: Drain voltage with turn on period of 48  $\mu$  S

voltage, red colour waveform shows gate source voltage, pink colour waveform shows the inductor current and blue current waveform shows the switch current.

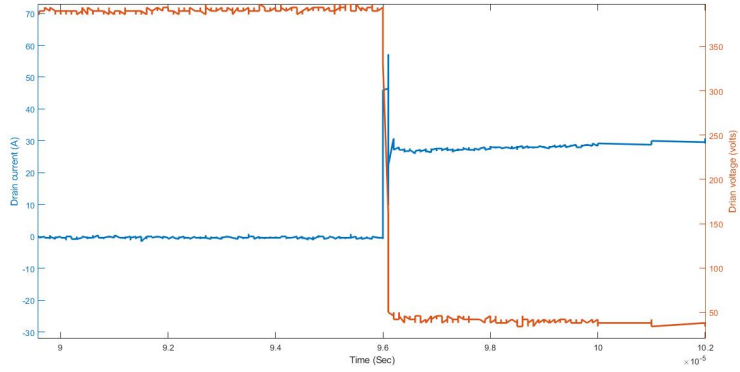


Figure 4.11: Drain current and drain voltage at turn on duration

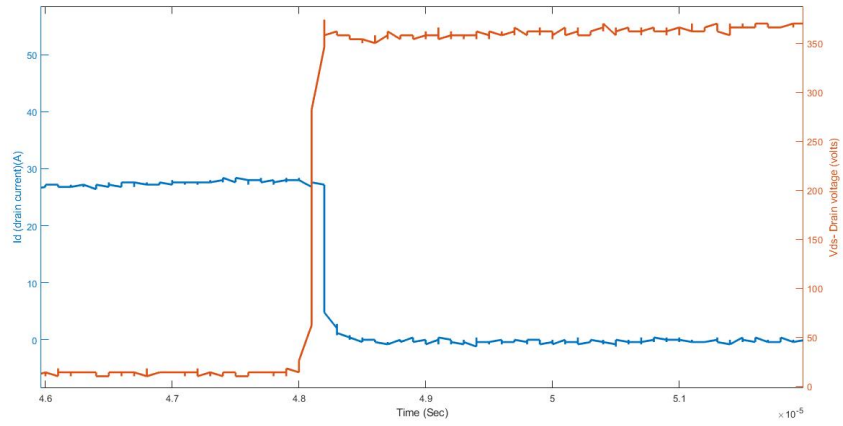


Figure 4.12: Drain current and drain voltage at turn off duration



Figure 4.13: IGBT turn on waveform for 50A inductor current

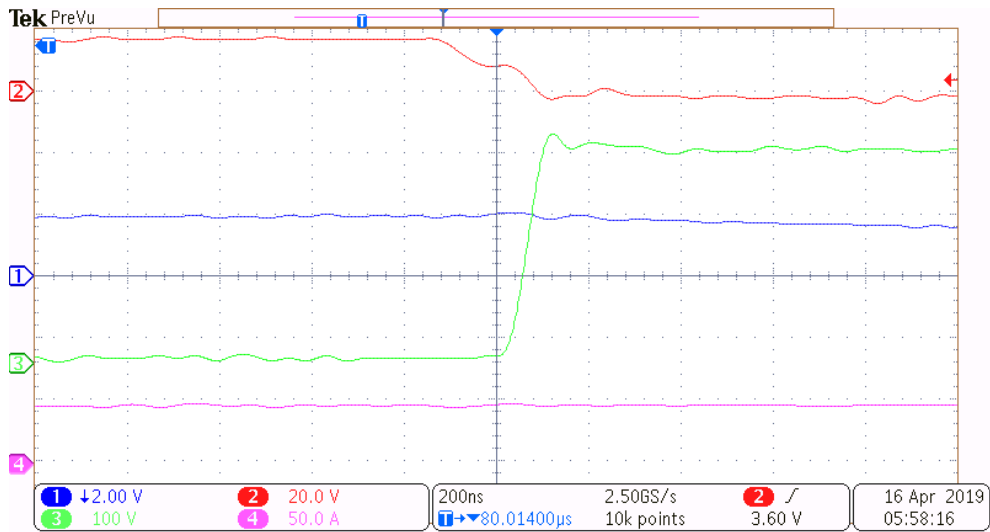


Figure 4.14: IGBT turn off waveform for 50A inductor current

## CHAPTER 5

### CONCLUSION

#### 5.1 Summary

Inverter used in EV is designed to handle the high peak current, because of which the size of inverter and losses increases thus, efficiency at light load reduces. Also, heat dissipation needs to be taken care.

For such high power switching inverters, IGBT devices are more advantageous than MOSFET due to its lower conduction loss and cost, but they have higher switching loss than MOSFETs which restricts their use for higher switching frequency applications. Using just WBG devices reduces the system losses but increases the overall cost of the system.

To reduce the cost and increase the energy efficiency, auxiliary inverter in parallel with main inverter can serve as effective solution. The auxiliary inverter is realized using WBG based devices. The WBG devices which have superior switching performance assists the Si-devices which have good conducting characteristics to minimize the overall losses improving the system efficiency. As per the proposed switching scheme, the WBG devices are used either for lower continuous load currents or to handle the high pulsating current. Therefore, the lower rated WBG devices suffice the need making the system cost effective. Simulation results using different driving cycles are done, which shows that EV inverter is mostly operated at light load condition. Using WBG device based auxiliary inverter at such point of operation helps to reduce the system losses. The energy efficiency using different configurations is compared. It can be inferred from the results that superior performance at affordable cost can be achieved by using auxiliary system compared to conventional Si-based or WBG based systems.

## **5.2 Future Work**

The vehicle modelling is done considering the constant battery voltage and temperature. Future work can focus on the modeling battery with consideration of temperature variation. Also focus would be given to resolve the issues faced while experimental validation and reduce the loop inductances in circuit mainly for GaN loops.

## APPENDIX

### COMPONENT DESCRIPTION OF DOUBLE PULSE TEST PROTOTYPE FOR AUXILIARY INVERTER CONFIGURATION

The prototype of double pulse test for auxiliary inverter is shown in Fig. A.1. It contains many parts i.e., high voltage side supply, isolated gate driver for Si IGBT and GaN, Isolated bipolar supply for both switches and switching devices.

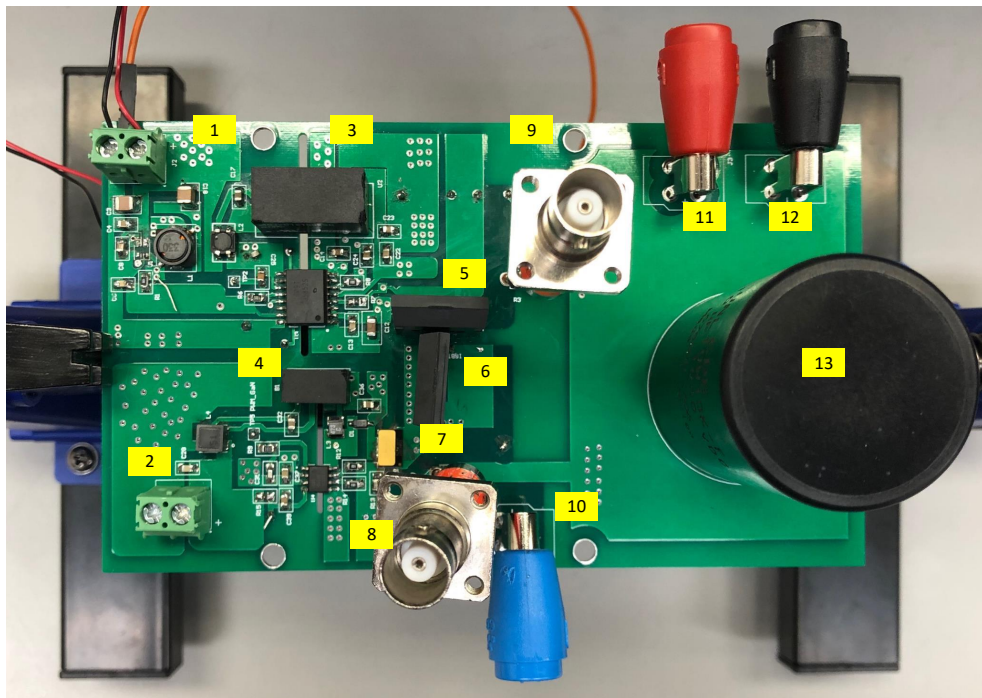


Figure A.1: Double Pulse test (DPT) prototype. 1. and 2. 12 volts and 5 volts power supply respectively, 3. Isolated DC-DC converter for 12 volts to 15/-5 volts supply, 4. Isolated DC-DC converter for 5 volts to 9 volts supply, 5. Top IGBT switch, 6. Bottom IGBT switch, 7. GaN switch, 8. shunt resistor for current measurement through GaN switch, 9. shunt resistor for current measurement through IGBT switch, 11 and 12. positive and negative DC bus supply, 13. DC link capacitor

The prototype is designed for 400V DC supply voltage (11,12) and hence switching device with capable of blocking 650 volts is considered. IKW30N65EL Si IGBT and GS66508T GaN switch is used (5,6,7). To illustrate the effectiveness of the proposed circuit, the lower

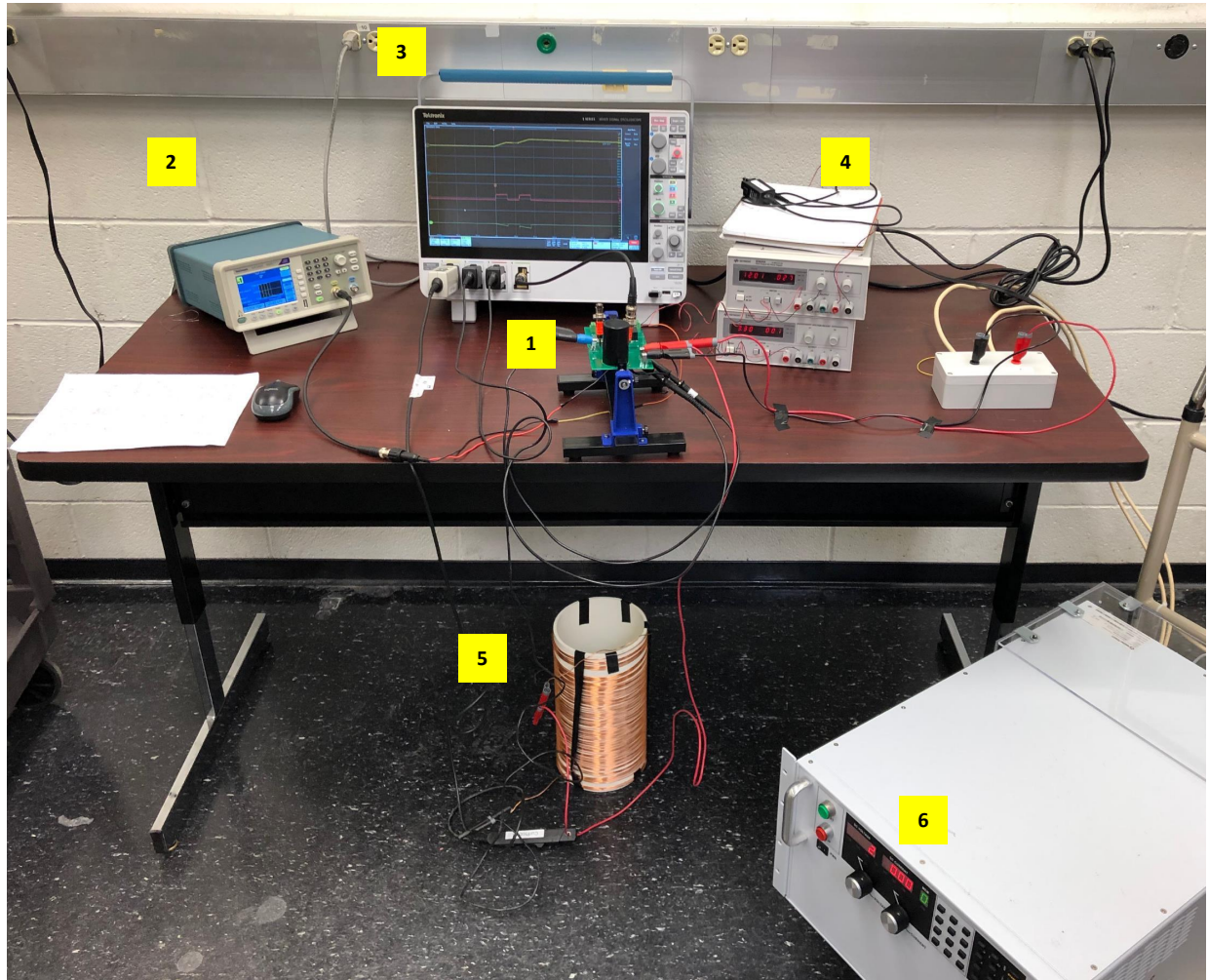


Figure A.2: Test set arrangement. 1. Double pulse test prototype, 2. Function generator, 3. Oscilloscope, 4. Power supply for gate driver part, 5. Load inductor, 6. 400 Volts DC power supply

IGBT and GaN switch are connected in parallel combination. As shown in Fig A.2, air core inductor is constructed with  $640\mu\text{H}$  and is used as inductive load for double pulse test. For double pulse test, the source and gate of upper Si IGBT is short circuited which is used for freewheeling purpose. The bottom and side view of prototype is shown in Fig. A.3 and A.4

The reference pulse are generated externally from function generator for Si IGBT and GaN device. Isolated DC-DC power supply MGJ2D122005SC is used for IGBT gate driver. It is capable of providing 15 and -5 volts from 12 volts input power supply which are

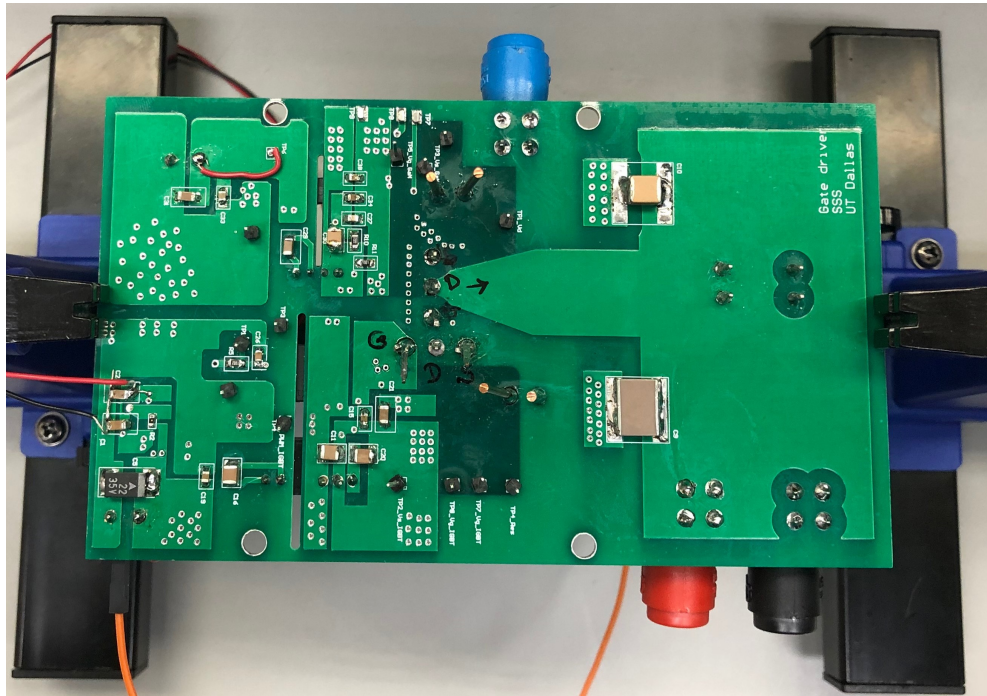


Figure A.3: DPT prototype for auxiliary inverter bottom view

recommend turn on and turn off voltages for Si IGBT. The 12 volts supply is also converted into 3.3 volts supply which is required for IGBT gate driver to provide pulse. 3.3 volts is generated on board. NKE0509SC is another isolated DC-DC power supply used for GaN switch. It is capable of providing 9 volts supply which is then converted into 6 and -3 volts as recommended in GaN systems application notes. To ensure that the given gate source voltage remains below the required voltage, zener diodes are used. Two 0.1 ohm resistances with low inductance from 'T & M research' is used to measure the current through both switches.



Figure A.4: DPT prototype for auxiliary inverter configuration side view

## REFERENCES

- [1] Costinett, P. D. (2017). Electric drive technologies for future electric vehicles-the university of tennessee. <http://web.eecs.utk.edu/~kaisun/ECE620/Fall12017/lectures/11082017-Costinett-EV.pdf>.
- [2] de Rooij David Reusch, A. L. J. S. M. (2014). *GaN Transistors for Efficient Power Conversion* (second ed.). John Wiley and Sons, Inc.
- [3] Deshpande, A. and F. Luo (2016). Comprehensive evaluation of a silicon-wbg hybrid switch. In *2016 IEEE Energy Conversion Congress and Exposition (ECCE)*, pp. 1–8.
- [4] Erickson, R. W. and D. Maksimovic (2001). *Fundamentals of Power Electronics* (2ed ed.). Springer.
- [5] Fiori, C., K. Ahn, and H. A. Rakha (2016). Power-based electric vehicle energy consumption model: Model development and validation. *Applied Energy* 168, 257 – 268.
- [6] Fiori, C. and V. Marzano (2018). Modelling energy consumption of electric freight vehicles in urban pickup/delivery operations: analysis and estimation on a real-world dataset. *Transportation Research Part D: Transport and Environment* 65, 658–673.
- [7] Jiang, Y., G. C. Hua, E. Yang, and F. C. Lee (1993). Soft-switching of IGBTs with the help of mosfets in bridge-type converters. In *Proceedings of IEEE Power Electronics Specialist Conference - PESC '93*, pp. 151–157.
- [8] Kishan, V. K., P. P. Puthra, and K. N. Reddy (2016). Paralleling of inverters with dynamic load sharing. In *2016 IEEE 7th Power India International Conference (PIICON)*, pp. 1–6.
- [9] Kumar, K., M. Bertoluzzo, G. Buja, and F. Ortenzi (2017). Quantitative analysis of efficiency improvement of a propulsion drive by using sic devices: A case of study. *Advances in Power Electronics 2017*, 1–10.
- [10] Kumar, K. and S. B. Santra (2018). Performance analysis of a three-phase propulsion inverter for electric vehicles using gan semiconductor devices. *IEEE Transactions on Industry Applications* 54(6), 6247–6257.
- [11] Mapelli, F. L. and D. Tarsitano (2012). Modeling of full electric and hybrid electric vehicles. In Z. Stevic (Ed.), *New Generation of Electric Vehicles*, Chapter 7. Rijeka: IntechOpen.

- [12] Mapelli, F. L., D. Tarsitano, and M. Mauri (2010). Plug-in hybrid electric vehicle: Modeling, prototype realization, and inverter losses reduction analysis. *IEEE Transactions on Industrial Electronics* 57(2), 598–607.
- [13] Mestha, L. K. and P. D. Evans (1989). Analysis of on-state losses in pwm inverters. *IEE Proceedings B - Electric Power Applications* 136(4), 189–195.
- [14] Mohan, N., T. M. Undeland, and W. P. Robbins (2003). *Power Electronics. Converters, Applications and Design* (third ed.). John Wiley and Sons, Inc.
- [15] Nikzad, M. R. and A. Radan (2009). Accurate modelling of traction inverter losses for efficiency calculation in parallel hybrid electric vehicles. In *2009 13th European Conference on Power Electronics and Applications*, pp. 1–7.
- [16] Ozpineci, B., M. S. Chinthavali, L. M. Tolbert, A. Kashyap, and H. A. Mantooth (2006). A 55 kw three-phase inverter with si igbts and sic schottky diodes. In *Twenty-First Annual IEEE Applied Power Electronics Conference and Exposition, 2006. APEC '06.*, pp. 7 pp.–.
- [17] Ozpineci, B. and L. M. Tolbert (2003). Characterization of sic schottky diodes at different temperatures. *IEEE Power Electronics Letters* 1(2), 54–57.
- [18] Ozpineci, B., L. M. Tolbert, S. K. Islam, and M. Hasanuzzaman (2001). Effects of silicon carbide (sic) power devices on hev pwm inverter losses. In *IECON'01. 27th Annual Conference of the IEEE Industrial Electronics Society (Cat. No.37243)*, Volume 2, pp. 1061–1066 vol.2.
- [19] Rabiei, A. (2013). *Energy Efficiency of an Electric Vehicle Propulsion Inverter Using Various Semiconductor Technologies*. Ph. D. thesis, Chalmers University of Technology.
- [20] Rabiei, A. (2015). *Efficiency Analysis of Drive-train for an Electrified Vehicle*. Ph. D. thesis, Chalmers University of Technology, Gothenburg, Sweden.
- [21] Sanjeev, P. and S. Jain (2013). Analysis of conduction and switching losses in two level inverter for low power applications. pp. 1–6.
- [22] SILICONIX, V. (2016). Power mosfet basics: Understanding gate charge and using it to assess switching performance. <https://www.vishay.com/docs/73217/an608a.pdf>.
- [23] Song, X., A. Q. Huang, M. Lee, and C. Peng (2015). High voltage si/sic hybrid switch: An ideal next step for sic. In *2015 IEEE 27th International Symposium on Power Semiconductor Devices IC's (ISPSD)*, pp. 289–292.
- [24] United States Environmental Protection Agency (US EPA) (2019). EPA vehicle chassis dynamometer driving schedules (DDS). <https://www.epa.gov/vehicle-and-fuel-emissions-testing/dynamometer-drive-schedules>.

- [25] Vindel, D., S. Haghbin, A. Rabiei, O. Carlson, and R. Ghorbani (2012). Field-oriented control of a pmsm drive system using the dspac controller. In *2012 IEEE International Electric Vehicle Conference*, pp. 1–5.
- [26] Wu, X., D. Freese, A. Cabrera, and W. Kitch (2015). Electric vehicles energy consumption measurement and estimation. *Transportation Research Part D: Transport and Environment* 34.
- [27] Yang, Y., S. M. Castano, R. Yang, M. Kasprzak, B. Bilgin, A. Sathyan, H. Dadkhah, and A. Emadi (2017). Design and comparison of interior permanent magnet motor topologies for traction applications. *IEEE Transactions on Transportation Electrification* 3(1), 86–97.
- [28] Zhang, H. and L. M. Tolbert (2009). Efficiency of sic jfet- based inverters. pp. 2056 – 2059.
- [29] Zhou, M., L. Zhao, Y. Zhang, Z. Gao, and R. Pei (2015). Pure electric vehicle power-train parameters matching based on vehicle performance. *International Journal of Control and Automation* 8, 53–62.

## **BIOGRAPHICAL SKETCH**

Saroj Sanjay Shinde was born in Maharashtra, India. She received her BE degree in Electrical Engineering from Lokmanya Tilak College of Engineering, Koparkhairane, Navi Mumbai, India affiliated with University of Mumbai in May 2017. After completing her bachelor's degree, she joined The University of Texas at Dallas to pursue Master of science in Electrical Engineering with power electronics and energy systems major. Since 2018, she has been working in the Power Electronics Lab under Dr. Gohil at UT Dallas. Her research interest focuses on renewable energy, medium voltage multilevel converter technology, wide band gap devices, and high-efficiency inverter.

# CURRICULUM VITAE

## SAROJ SANJAY SHINDE

Dallas, Texas

### OBJECTIVE

---

Seeking a challenging position in Power Electronics and Renewable Energy systems.

---

### EDUCATION

---

- The University of Texas at Dallas**, Richardson, TX **GPA: 3.76/4.0**  
**M.S. in Electrical Engineering** (May 2019)  
Coursework: Power Electronics, Microprocessor Systems, Renewable Energy Systems and Distributed Power Generation Systems, Control Modeling and Simulation in Power Electronics, Adjustable Speed Motor Drives, Advance power converters, Analog Integrated Circuit Analysis and Design
- The University of Mumbai**, Maharashtra, India **CGPI: 9.13/10.0**  
**B.E. in Electrical Engineering** (May 2017)

### SKILLS

---

- Operating Systems : Windows XP/10, Ubuntu Linux  
Software : PLECS standalone, MATLAB/Simulink, LT SPICE, Altium, P-SPICE, PSIM, LabVIEW, Microsoft Office, Code Composer Studio, Auto Cad, ANSYS Fluent, CADENCE CAD  
Laboratory experience : Hands on experience of SMD component soldering, PCB circuit design and testing using multimeters, power supplies & oscilloscope, familiar with testing of 80 kw 3 phase inverter  
Programming Languages : C++, C, assembly language (8085)  
Core Competencies : Quick learner, analytical, statistical & problem-solving skills, innovative, self-initiative and organized

### PROFESSIONAL EXPERIENCE

---

- ❖ **Graduate Research Student**, University of Texas, Dallas (May 2018 – Present)  
Working in Power Electronics Lab on efficient and cost-effective parallel inverter configuration for increasing efficiency of electric vehicle inverter using wide band gap devices (SiC, GaN). Designing double pulse test circuit. Learned schematic and PCB designing in ALTIUM software. Simulated different DC-DC and AC-DC converters in PLECS, MATLAB, LT-SPICE and P-SPICE software for estimating device losses.
- ❖ **Student Lab worker**, Texas Analog Center Of Excellence, (Mar 2018 – May 2018)  
Worked on project - 'Analysis of noise trends as a function of process node'. Review of IEEE papers and evaluation was done.
- ❖ **Vacation Trainee**, Tata Power Co. Ltd., Trombay Thermal Power Station, Shahad, (Jun 2015 – Jul 2015)  
Learned overview of thermal power stations - 500MW, 150MW & 250MW and studied detailed working and construction of dummy switchyard.

### ACADEMIC PROJECTS

---

- Advance power converters design using PLECS software** (Dec 2018)
- Designed electric vehicle charger, focusing on PFC stage with supply side current THD less than 5%.
  - Designed Vienna and Delta rectifier for 10kw telecom rectifier. Studied dual active bridge and resonant converters.
  - Evaluated performance of T, H5, Heric and recent Transformer less inverter structure for 5.6 KW.
  - Designed and simulated 4.4 KW, 230V single phase grid connected PV system using H5 inverter topology. Designed SOGI-PLL, Incremental conductance MPPT and current control scheme using c-script block in PLECS. Calculated power losses in semiconductor devices.

**Designed DC converters using LT-SPICE**

(Dec 2017)

- Designed Buck converter, Boost converter, Buck Boost converter, Flyback, Forward converter using LT-Spice software.
- Performed loss calculation, efficiency calculation of converters, also selected various components required for converters with proper required ratings

**DC motor control using MSP430 Board**

(Dec 2017)

- Fabricated and programmed 3 phase brushless DC motor control using MSP430 board (C language). Project is designed using PWM principle, where speed of motor is controlled by varying the duty cycle of the pulse.

---

**PUBLICATION**

---

[1] Saroj S. Shinde, Vaibhav U. Pawaskar, Surabhi S. Hatagale, Snehal P. Sonawane and Madhwi Kumari. 'Ansys simulation of portable vertical axis wind blades for urban rooftop green energy'. Industrial Engineering Journal, June 2017

---

**LEADERSHIP ACHIEVEMENTS**

---

- **Chairperson** - **IEEE** student Committee Lokmanya Tilak college Engineering (STB:61251)  
(Aug 2016- May 2017)

---

**REFERENCE**

---

Prof. Ghanshyamsinh Gohil (Assistant Professor,UTD)

E-mail: [ghanshyam.gohil@utdallas.edu](mailto:ghanshyam.gohil@utdallas.edu) , Web: <http://utdallas.edu/~ghanshyam.gohil/>